Comparison of Diagnostics for Determining Z Pinch Centroid in the ZaP-HD Experiment

Timothy Lloyd

A thesis
submitted in partial fulfillment of the
requirements for the degree of

Master of Science in Aeronautics and Astronautics

University of Washington

2022

Reading Committee:

Uri Shumlak, Chair

Justin Little

Program Authorized to Offer Degree:
Aeronautics and Astronautics

University of Washington

Abstract

Comparison of Diagnostics for Determining Z Pinch Centroid in the ZaP-HD Experiment

Timothy Lloyd

Chair of the Supervisory Committee:
Dr. Uri Shumlak
Aeronautics and Astronautics

A Z-pinch configuration plasma has been theoretically shown to be a viable fusion energy source. By applying radially sheared flow, the Z pinch instabilities can be mitigated. In the process of stabilizing the pinch for long pulses, new research opportunities arise in studying this equilibrium plasma. One area of research is attempting to determine the centroid location of the pinch in space. Diagnostic tools are available that can measure various qualities and parameters of the plasma, but no tools are effective in directly measuring the centroid location. Instead, these diagnostics measure the plasma and, using several assumptions, are able to make an inference about the centroid. This paper examines three different diagnostic tools in their accuracy and relevance for determining centroid location. A Kirana fast-framing camera is used to measure visible line emissions from neutral gas in the vacuum chamber. A Helium-Neon laser interferometer is used to measure electron number density along the vertical axis and throughout the pinch. Finally, a set of magnetic field probes are able to measure the magnetic field at the cylinder walls and reduce the raw magnetic field data to centroid location through a simple serious of equations. The Kirana is the most consistent in determining pinch location, but is susceptible to wayward light reflections or over saturation of the detector. The interferometer is roughly accurate during the quiescent period of the plasma. It does however follow the velocity of the centroid as it moves throughout the vacuum chamber. The magnetic field probe data are accurate during the quiescent region because of the current assumptions and equations being used.

TABLE OF CONTENTS

LIST OF FIGURES

LIST OF TABLES

ACKNOWLEDGMENTS

I would like to give a special thanks to Uri Shumlak for his thoughtful advice and guidance provided throughout my time at the University of Washington. I would also like to thank Aqil Khairi for his help in training me to use the ZaP-HD machine, Aria Johansen for helping me to understand all the complexities of plasma physics, Bennett Diamond for providing his unique problem solving advice on computer codes, and Harry Furey-Soper for his excellent design and fabrication of the next iteration of Kirana periscope.

Chapter 1

INTRODUCTION

As energy demand continues to rise across the globe, countries are looking for more stable, clean sources of electricity. Renewable energy sources, such as wind and solar, can satisfy some of the demand, but it is clear that nuclear power will play a major role in meeting the energy needs of the future. Nuclear fission energy, although safe and reliable, tends to have a negative public opinion and has faced several political setbacks over the last few years. Now researchers are turning more towards nuclear fusion as a viable source of energy. Nuclear fusion holds the potential for safe, clean, and almost limitless energy.

Nuclear fusion proves to be difficult, however. Nuclear fusion energy requires enormous amounts of energy to run, mainly in the form of heating plasma and running large magnets to confine plasma. While fusion can be accomplished, the energy input has always been greater than the energy output. Several configurations have been invented in order to confine and heat the plasma, including the tokamak[1], the spheromak[15], and the Z pinch. What differentiates the Z pinch from other configurations is its simplicity and lack of external magnets. However, these positive characteristics are balanced out by multiple types of instabilities within the plasma. Multiple papers from the 1940's and 50's predicted and outlined the instabilities inherent in the Z-pinch configuration. Although these instabilities are still a problem today, they can be mitigated with the addition of radial sheared flow in the plasma[10]. This demonstration in the ZaP lab at the University of Washington has lead to the development of other sheared flow Z pinch configurations, such as ZaP-HD and FuZE, the latter of which is working on nuclear fusion specifically.

The Z pinch can be applied to other scientific areas as well. Although not proven, it has been theorized that a Z-pinch propulsion device could be implemented onto spacecraft or satellites for long duration missions requiring low thrust and high efficiency applications. If sustainable nuclear fusion becomes viable, the Z pinch could be a multipurpose engine,

supplying both bus power and thrust for a space mission.

As the current experiments continue to development and the breakthrough of sustainable nuclear energy approaches, it is vital to develop and characterize diagnostic tools that will enable researchers to validate their hypothesis or findings. A Kirana fast-framing camera will be used to measure visible light emission from excited, neutral hydrogen gas. This camera will be able to view the pinch along two axes and along the entire pinch length. An interferometer will be used to measure electron number density along one axis. Finally, a set of magnetic field probes in the machine will measure the magnetic field caused by the current density. None of these tools directly measure the plasma centroid, but assumptions and methods can be developed to make inferences about the location of the plasma centroid. This thesis attempts to merge multiple diagnostic tools commonly used in the field of plasma, and find relationships between them and locating the centroid of the plasma pinch within ZaP-HD.

1.1 History of the Z Pinch

The first Z pinch was first discovered by accident by Martinus van Marum in 1790. This was done when he discharged 100 Leyden jars into a wire, which caused an explosion. The Z pinch was not well understood until 1905 when Pollock and Barraclough investigated a crushed lightning rod after it had been struck by lightning. Willard Harrison Bennett was the first to come up with the pressure equilibrium equation that is now used today for analysis of Z pinches. Soon after, Thompson and Blackman submitted the first patent for a toroidal Z-pinch thermonuclear fusion reactor[3]. Their design intended to inject the deuterium plasma in the toroidal direction. The induced magnetic field would be in the poloidal direction, and the resulting Lorentz force would point radially inwards. This configuration would allow the plasma to be heated up without interacting with the walls. An additional magnetic field was included in the vertical direction to prevent outward drift of the plasma. The heating would be accomplished via radio waves fed into the plasma through small holes along the outside of the toroid.

In the 1950's, multiple papers came out detailing the instabilities associated with a Z-pinch plasma. The first was published in 1954 by Kruskal and Schwarzschild. In this

paper, they outlined possible instabilities of the Z pinch using MHD equations[6]. In 1956, Kurchatov proved these instabilities experimentally through pulsed discharges of current and plasma. The initial rise in popularity of Z pinches would be short lived, however. Due to the limitations in technology and understanding at the time, researchers were not able to make any significant progress in controlling the instabilities. At the same time, Tokamak fusion devices showed much promise, and quickly overtook Z-pnch devices as the predominant fusion research focus[9].

1.2 Z-Pinch Applications

1.2.1 Z-Pinch Fusion

Thompson and Blackman's original design of their toroidal fusion reactor used only deuterium as a fuel source. This reaction would release heat, along with an isotopes of helium and either a proton or neutron. Although this deuterium a viable fuel source, it was discovered that using a combination of deuterium and tritium allowed for easier initiation of reactions and produced more energy per reaction. Shown below are the different reactions that can occur between deuterium, tritium, and helium.

$$^{2}_{1}H + ^{2}_{1}H \rightarrow ^{3}_{2}He + ^{1}_{0}n + 3.27MeV \tag{1.1}$$

$$^{2}_{1}H + ^{2}_{1}H \rightarrow ^{3}_{1}H + ^{1}_{1}p + 4.03MeV \tag{1.2}$$

$$^{2}_{1}H + ^{3}_{2}He \rightarrow ^{4}_{2}He + ^{1}_{1}p + 18.4MeV \tag{1.3}$$

$$^{2}_{1}H + ^{3}_{1}H \rightarrow ^{4}_{2}He + ^{1}_{0}n + 17.59MeV \tag{1.4}$$

Equations 1.1 and 1.2 are the possible reactions that can occur as a result of deuterium fusion. These two are generally not used as they yield low amounts of energy compared to deuterium-tritium reactions. Equation 1.3 is a secondary reaction that can occur as a result of the first equation 1.1. The last equation shows the reaction that occurs during the more popular deuterium-tritium fusion process. The deuterium-helium-3 reaction may appear more attractive upon first glance because of its extra 1 Mev energy gain over deuterium-tritium. However, the process to heat up helium-3 to fusion temperatures is much higher

than that of hydrogen isotopes, resulting in a lower net energy output. Deuterium is a popular fuel choice not only because of its fusion properties, but also because it is so abundant. Deuterium is naturally occurring in seawater, with approximately 1 out of every 5000 to 6000 atoms of hydrogen being deuterium. This means that 1 gallon of seawater could produce as much energy as 300 gallons of gasoline[7].

The other fuel reactant, tritium, is not so abundant in nature. It is only produced in small quantities when galactic cosmic rays interact with the atmosphere or very rarely found deep within earth's crust. However, tritium can be manufactured from the nuclear fusion process in a process called tritium breeding. In order to do this, nuclear reactors are lined with a layer of a lithium compound, typically lithium titanate or lithium orthosilicate[4]. This layer is often referred to as a breeding blanket or a lithium blanket. Tritium breeding works by harnessing the freed, energetic neutron released from the deuterium-tritium reaction. The neutron collides with the lithium atoms, releasing a helium and a tritium atom. This new tritium atom will then be used to fuel the next reaction.

1.2.2 Z-Pinch Propulsion

The current area of interest for Z pinch leans heavily on producing sustainable nuclear fusion reactions. However, the Z-pinch configuration can be modified to produce thrust in a relatively small, lightweight package. Furthermore, a Z-pinch thruster that could produce fusion reactions would double in function; it could produce energy for the spacecraft while also providing the thrust necessary for the mission.

To adapt the current ZaP-HD experiment to a thruster design would be relatively straightforward. The configuration is already linear and it could be scaled up or down to meet the needs of the spacecraft. The major difference would be a change in the end of the outer electrode. Instead of the typical end wall that impinges the plasma flow, the end wall would be removed in favor of a nozzle. Some of the fusion power would be taken by a power converter to power the rest of the spacecraft and continue to run the propulsion system. The rest of the plasma would be exhausted out of the nozzle to create the thrust. As the plasma cools, it will recombine and become a neutral exhaust. This neutrality eliminates

the need for a hot cathode, or other neutralizing source, like many other space propulsion systems require[11]. It has also been theorized that using a different set of fusion reactants than the typical deuterium-tritium could further reduce the mass of the propulsion system. If a system were to utilize a combination of $D - {}^3He$ or $p - {}^{11}B$, the neutrons created per reaction could either be reduced or eliminated completely, respectively.

Reducing the number of neutrons produced is an important concern for future deep space missions utilizing nuclear power. Energetic neutrons released from nuclear reactions can cause serious damage to the crew or to other components of the ship. As a result, radiation shielding will need to be implemented to mitigate this. However, reducing the neutrons emitted would allow for little to no shielding on the reactor and would help keep the spacecraft safe.

1.3 Z-Pinch Plasma and Instabilities

A Z-Pinch plasma is named for its axial current along the z axis. For this configuration, there exists a balance between the outward pressure from the plasma and the inward pointing Lorentz forces. Below, equation 1.5 describes this relationship.

$$\frac{dp}{dr} = -J_z B_\theta \tag{1.5}$$

Ampere's Law,$\nabla \times \vec{B} = \mu_0 \vec{J}$, describes the relationship between magnetic field and current density. In cylindrical coordinates, this becomes

$$\frac{1}{r}\frac{d}{dr}(rB_\theta) = \mu_0 J_z \tag{1.6}$$

Assuming a thermalized plasma, that is $T = T_e = T_i$, equations 1.5 and 1.6 can be combined to describe a one dimensional Z pinch[13].

$$-\frac{d}{dr}(p + \frac{B_\theta^2}{2\mu_0}) = \frac{B_\theta^2}{\mu r} \tag{1.7}$$

The left hand side of the equation encompasses the outward plasma pressure as well as the magnetic pressure. The right hand side includes a tension term that arises from the curvature of the azimuthal field.

Early research into Z-pinch plasma was slowed because of an inability to mitigate instabilities in the plasma. These instabilities are caused by small perturbations away from equation 1.7, which continue to grow rapidly until the pinch terminates. The two instabilities that the ZaP-HD experiment are concerned with are the sausage and kink instabilities, which are associated with the $m = 0$ and $m = 1$ modes, respectively. The $m = 0$ mode instability occurs when a perturbation causes one region of the pinch to have a slightly smaller radius than the surrounding pinch. The plasma current density is higher here than the rest of the pinch, resulting in a stronger magnetic field compressing the pinch further, as seen on the left side of Figure 1.1. This positive feedback loop continues until the pinch has compressed so much that it becomes severed. The $m = 1$ mode instability occurs when a perturbation pushes a portion of the pinch off-center, which results in a bend, as seen on the right side of Figure 1.1. This causes the magnetic field strength to be higher on the inside bend than the outside. This difference in magnetic field strength continues to build until the pinch is bent enough to sever it.

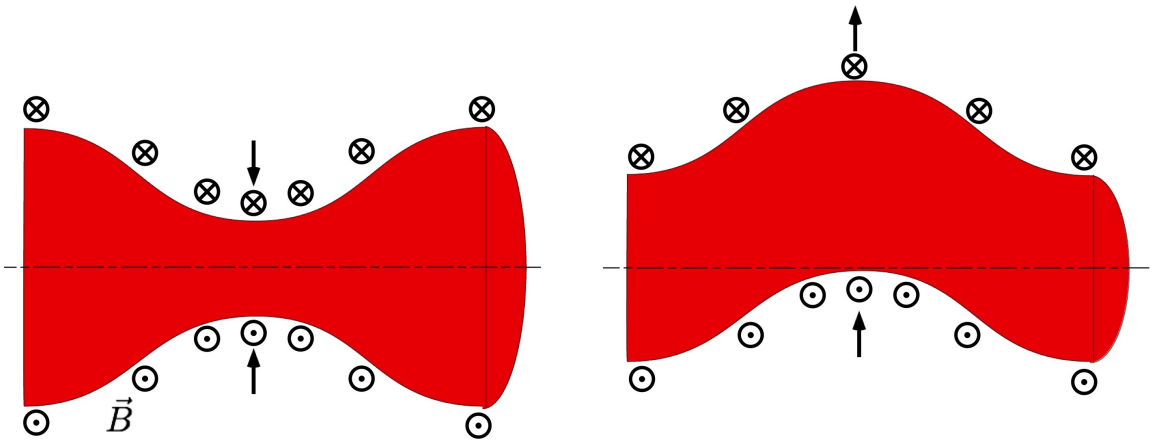

Figure 1.1: Instability modes commonly found in a z-pinch plasma. The left side of the image shows the $m = 0$ sausage instability, while the right side shows the $m = 1$ kink instability[2]

Several attempts have been made to stabilize the Z pinch. One method included the addition of a external, longitudinal magnetic field so that the plasma would gyrate around the axial field lines[8]. However, this added complexity and also resulted in additional losses to the electrodes. Another method tried to stabilize the $m = 1$ instability by placing a conducting wall within 20% of the pinch radius. This would induce currents in the wall that could theoretically stabilize the plasma. This proved to be unfeasible for fusion applications as the heat loss to the walls would be excessive.

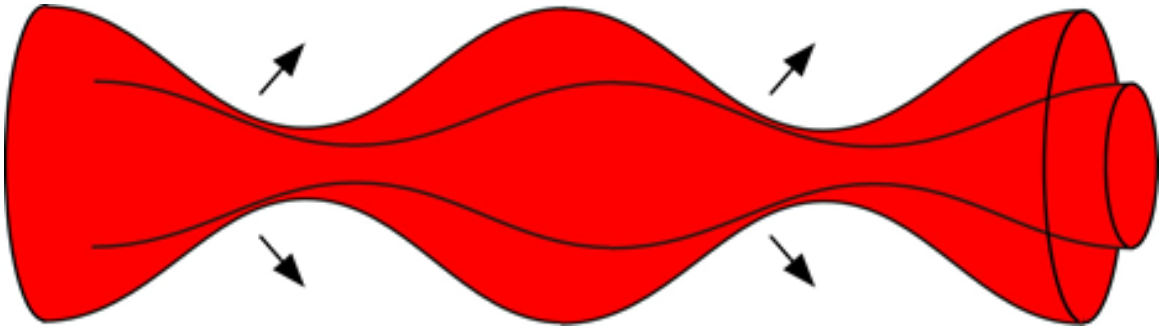

Figure 1.2: This diagram shows how radially sheared flow in a Z-pinch plasma has the ability to reduce and mitigate the $m = 1$ instability[5]

The $m = 1$ instability can be somewhat mitigated through the used of sheared axial flow. In a Z pinch with this configuration, axial flow velocity varies with radial position away from the center[10][12]. Figure 1.2 provides a simple visual example for how sheared flow stabilization occurs. In a numerical simulation, radial sheared flow conditions were examined and deemed to be effective at stabilizing the pinch at sufficiently large differential speeds. Figure 1.3 outlines the trend for radial sheared flow stabilization criteria. For a Z-pinch plasma to be stabilized, the radial differential velocity must satisfy

$$\frac{dV_z}{dr} \geq 0.1kV_A$$

where k is the wave number, and V_A is the Alfvén velocity, given by

$$V_A = \frac{B}{\sqrt{\mu_0 \rho}}$$

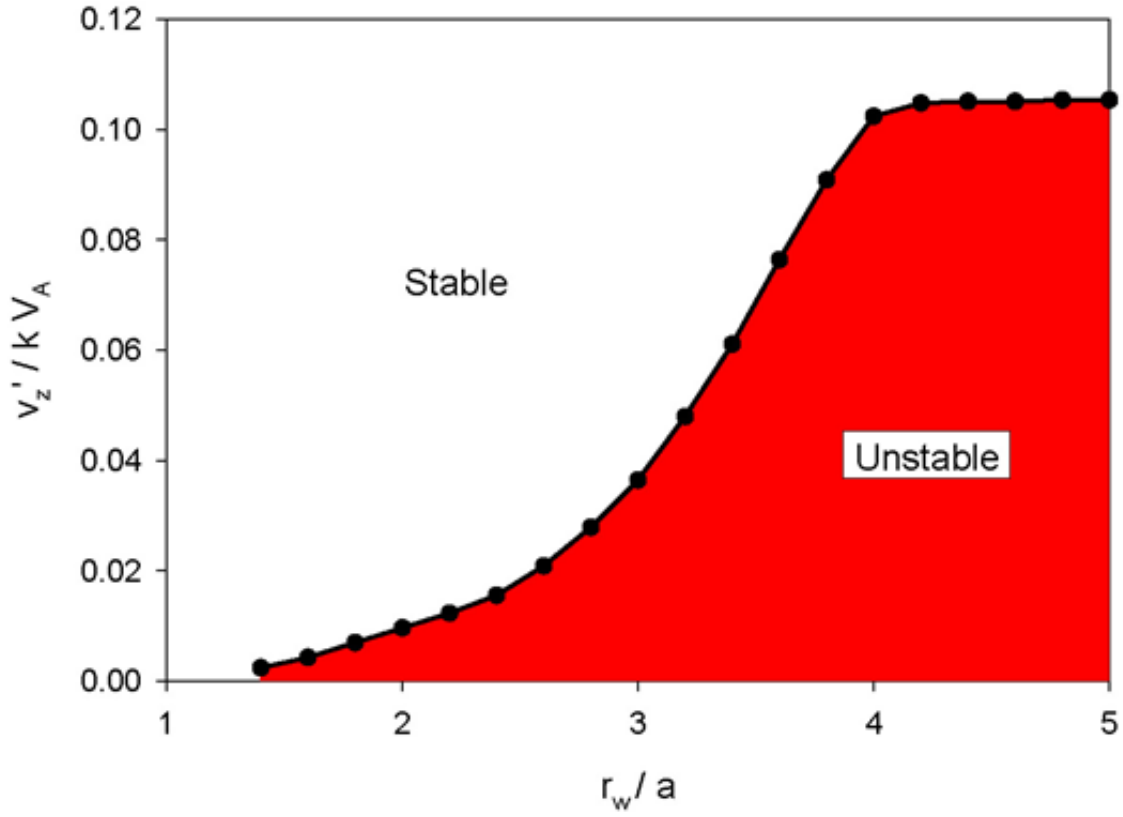

Figure 1.3: This plot highlights the radial sheared velocity required for stability in a Z-pinch plasma[5]

Chapter 2

THE ZAP-HD EXPERIMENT

The ZaP-HD experiment began at the University of Washington as the successor to the original ZaP experiment. One way that ZaP-HD improves on the previous ZaP configuration is through the addition of a third electrode, designed to improve plasma acceleration and compression. The third electrode allows for separate voltage levels between the compression and acceleration regions as well as variable timing for voltage discharge between the outer and inner electrodes. Voltage discharge is accomplished via external capacitor banks. The acceleration region is responsible for ionization of the injected gas and accelerating it towards the compression region downstream. This region includes the middle and inner electrodes as well as gas vales responsible for puffing in the neutral gas. Gas injection is controlled by 9 Parker fast puff valves, with 8 being positioned azimuthally around the middle electrode and one more positioned inside the inner electrode. The outer and inner valves are connected to separate control circuits, allowing for separate timing of gas puffs. The acceleration region is 1 meter long and goes from the azimuthal gas valves to the tip of the nose cone on the inner electrode. The compression region is responsible for creating the Z pinch and includes several diagnostic tools for monitoring the pinch. This region includes the outer and inner electrodes and are similarly controlled by and separate, external capacitor bank. This region extends from the tip of the nose cone to the end wall of the outer electrode, for a total of 50 centimeters. There 5 centimeter wide windows on the sides and top of the vacuum chamber in the compression region. The windows are made of fused silica and have an infrared reflective coating. There are several diagnostic tools used at multiple axial locations which use a naming prefix of either 'P' or 'N' to designate the compression region or acceleration region, respectively. These values are also measured with reference to the nose cone. So, a measurement at 'P15' would indicate 15 centimeters downstream from the nose cone, while 'N10' would indicate 10 centimeters upstream from the nose cone.

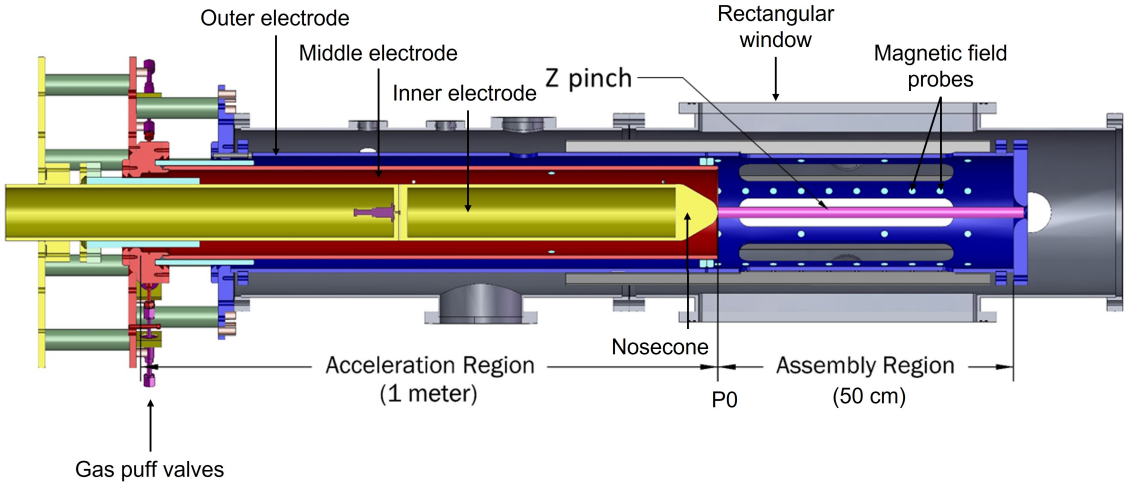

Figure 2.1: The ZaP-HD device is equipped with two coaxial electrodes with their own power supplies. The neutral gas is injected in between the inner and middle electrodes, where it is ionized and accelerated towards the assembly region. The outer electrode is able to compress the plasma into the Z pinch. ZaP-HD is also equipped with several magnetic field probes within the outer electrode[2]

2.1 Pinch Formation

The first step to creating a plasma needed for the pinch is to inject a neutral gas into the acceleration region. Hydrogen is a cheap and easily accessible option, but gasses such as hydrogen isotopes or methane may also be injected depending on the application. Once gas is injected, the first set of capacitor banks are discharged to begin ionizing the gas. The slab of plasma is now accelerated through the $\vec{J} \times \vec{B}$ force downstream in what is known as the snowplow effect. Figure 2.2 provides a diagram of how a coaxial plasma accelerator operates.

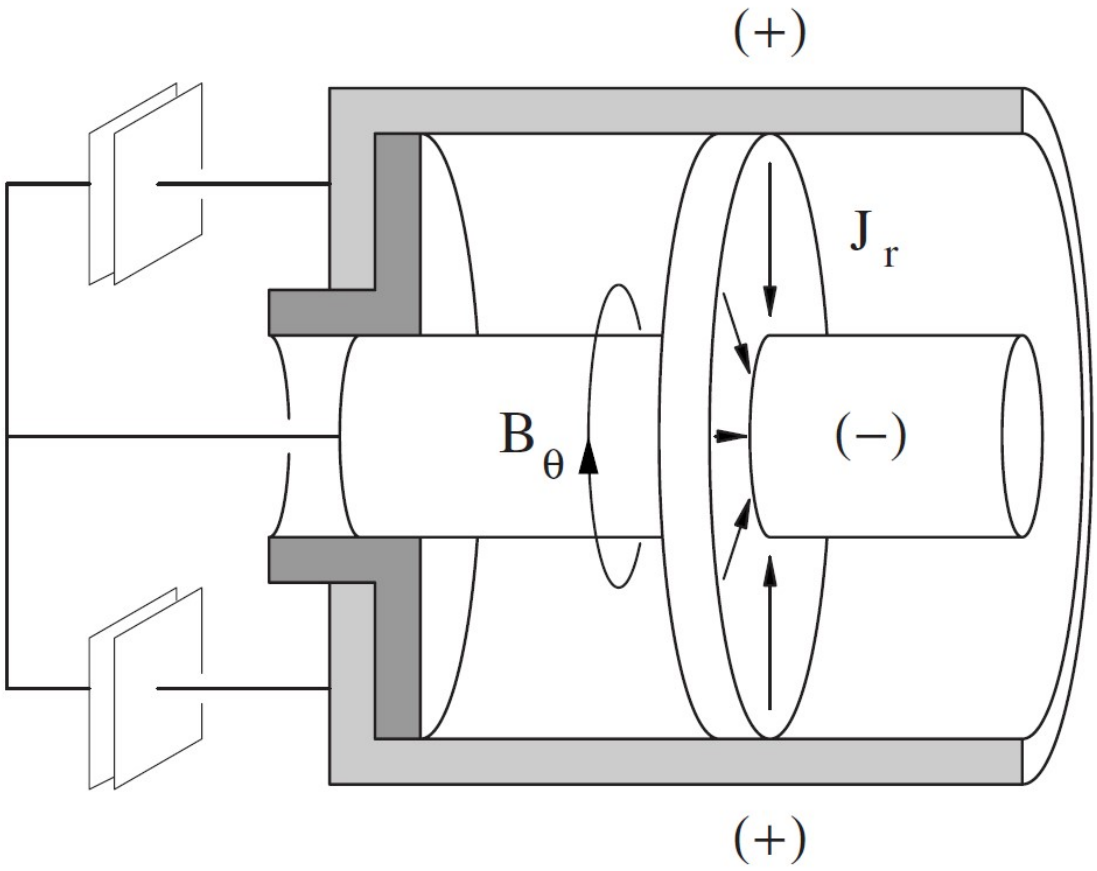

Figure 2.2: This picture shows a simple diagram of how the plasma accelerates in a coaxial configuration, also known as a snowplow[14]. The electric field causes the plasma current to point in the direction of the inner electrode. The Lorentz force causes a net force to the right, causing the snowplow plasma to move down the machine.

Once the snowplow moves far enough downstream, the second set of capacitors are discharged to increase the plasma current and form the pinch in the compression region. The pinch will be sustained until the gas source is depleted, the capacitors stop providing current, or the instabilities grow too large. Below is a series of pictures showing how the plasma pinch forms after being initially accelerated.

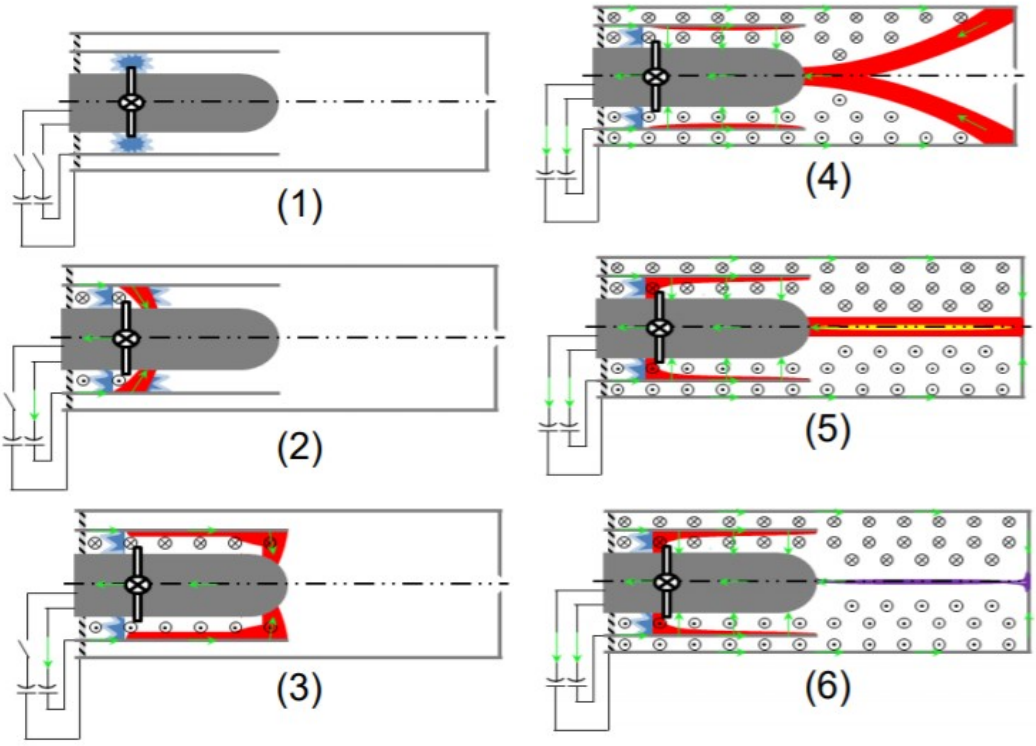

Figure 2.3: The above pictures show how the ZaP-HD machine forms the Z pinch[16]. Figures 1-3 show the neutral gas being ionized and forming a snowplow as it is accelerated. Figures 4-6 show the plasma collapsing in towards the center as the second set of capacitors are discharged. The plasma is sustained as long as gas is supplied, the capacitors are discharging, and the pinch does not succumb to instabilities[2]

2.2 Diagnostics

2.2.1 Kirana

A Kirana high-speed imaging camera was used extensively throughout this experiment to help characterize pinch location, shape, and instabilities. This model records 180 frames at speeds of up to 5 million frames per second with exposure times as low as 100 nanoseconds at a resolution of 924x768 pixels. The lens used was a Nikon AF Nikkor lens, with a focal length range of 80 to 200 millimeters. In addition, an Altura ND4 neutral density filter was used to reduce the intensity of incoming light by 75%. All shots in this analysis recorded visible light, but a phosphor intensifier is also available to view the ultraviolet spectrum.

The Kirana camera is mounted on a tripod for ease of adjustment and handling. A periscope mount is also used to allow the Kirana to view a simultaneous view of the top and side of the pinch in the compression region. The periscope is composed of three mirrors and a 3D printed mounted system that can slide onto the outer rails of the experiment. All shots analyzed in this paper were obtained with the Kirana perpendicular to the viewing windows.

2.2.2 B Field Probes

The probes installed on the ZaP-HD machine do not directly measure magnetic field. Instead they measure voltage through a wire caused by a changing magnetic field, through which the absolute magnetic field can be determined. Faraday's Law describes the relationship between changing magnetic flux through a surface, the electric field running through a conductive material at the edge of the surface, and the voltage induced through the conductive material.

$$\int \frac{d\overrightarrow{B}}{dt} \cdot d\overrightarrow{S} = -\oint \overrightarrow{E} \cdot d\overrightarrow{l} = -V_i$$

The equation above relates a time dependant magnetic field to an induced voltage in a single loop wire. The voltage is also related to the number of loops, N, that circle the edge of the surface with area, A, as described below:

$$-N \int \frac{d\overrightarrow{B}}{dt} \cdot d\overrightarrow{S} = V_i$$

Integrating with respect to time and solving for the magnetic field yields the following:

$$B_{avg} = \frac{1}{NA} \int_0^t V_i \, dt$$

The ZaP-HD experiment is equipped with several probes at multiple axial locations, both in the compression and acceleration regions. There are 8 probes every 15 centimeters downstream from the nose cone (P0, P15, P30, etc.) and 4 probes installed every 5 centimeters in between the previously mentioned locations (P5, P10, P20, etc.). All magnetic field probes are placed within the outer electrode. The magnetic field probes allow for precise analysis of the $m = 0$ and $m = 1$ modes of the plasma, as well as for determining plasma centroid location.

2.2.3 Interferometry

Interferometry is the process by which the principal of superposition and interference from overlapping waves are used to analyze a system. In the ZaP-HD experiment, a Mach-Zender Heterodyne Interferometry setup with a Helium-Neon (HeNe) steady state laser is used to determine the density of the pinch. The Mach-Zender setup involves splitting a beam into a scene beam and a reference beam. The scene beam passes through the system of interest, which is the plasma pinch in this case. The reference beam will completely bypass the plasma and will recombine with the scene beam after the plasma pinch. The scene beam will experience a phase shift as it passes through the plasma as a result of the change in refractive index.

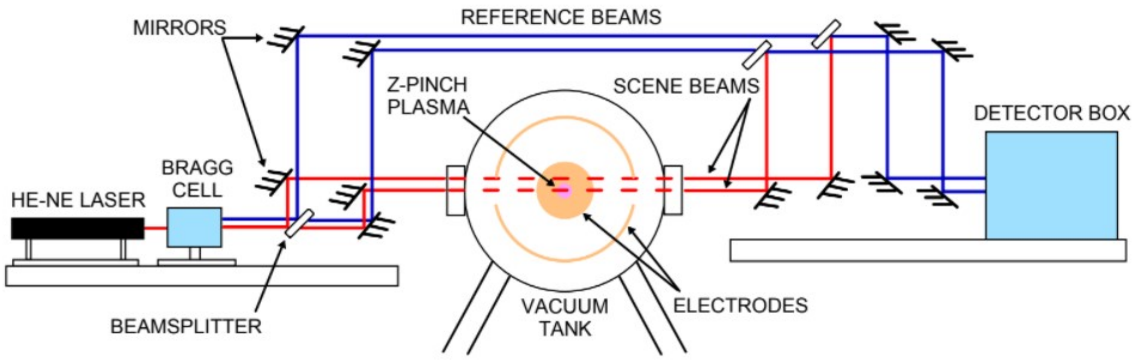

Figure 2.4: The original beam is split by an acousto-optic modulator, where two beams emerge. One beam has the original frequency while the other is shifted by a known frequency. The scene beam passes through the plasma while the reference beam passes over the plasma. The beams are recombined at the detector[5]

Assuming that the pinch is a cold, magnetized plasma, we can use the dispersion relation from the Appleton-Hartree dispersion equation.

$$N^2 = 1 - \frac{X(1-X)}{1 - X - \frac{1}{2}Y^2\sin(\theta) \pm ((\frac{1}{2}Y^2\sin(\theta))^2 Y^2\cos(\theta)^2)^{\frac{1}{2}}}$$

For a perpendicular propagating wave or for a negligible magnetic field, the above equation can be reduced down.

$$N^2 = 1 - X = 1 - \frac{\omega_p^2}{\omega^2}$$

We can determine the total phase lag using the equation

$$\phi = \int kdl = \int N\frac{\omega}{c}dl$$

A significant portion of the above line integral is outside the plasma pinch. In addition, the reference beam has a phase lag that is not precisely known. To mitigate this, we can look at the in phases between the scene and reference beams.

$$\Delta\phi = \int (k_{plasma} - k_0)dl = \int (N-1)\frac{\omega}{c}dl$$

This equation assumes vacuum conditions outside of the chamber and defines $k_0 = \omega/c$. We can also rewrite the dispersion relation above to

$$N^2 = 1 - X = 1 - \frac{\omega_p^2}{\omega^2} = 1 - \frac{n_e}{n_c}$$

where $n_c \equiv \omega^2 m\epsilon_0/e^2$ is known as the cutoff density. For $n_e \ll n_c$, we can approximate N as $N \approx 1 - \frac{1}{2}(n_e/n_c)$. Substituting this back into our above integral allows us to solve for the average chord density

$$\Delta\phi = \frac{\omega}{2cn_c}\int n_e dl$$

The above equation describes how the phase shift between the two beams is related to the line integrated electron charge density of the plasma.

Heterodyne involves using beams of slightly offset frequencies that are mixed. Once the beams are mixed, they create an interference pattern at the same frequency as the offset frequency. The offset frequency is produced by an acousto-optic modulator (AOM), also known as a Bragg Cell. A known frequency is sent to the AOM which vibrates some physical medium inside. As the beam passes through the vibrating medium, it is split into multiple beams and dispersed. One beam that emerges from the cell has the original frequency, while the others are now frequency shifted by the known input frequency. The recombined beams are sent into a detector box that will then send the intensity signal to the digitizer racks. The response time of the detector is much slower than the laser frequency, resulting in the detector averaging the high frequency term and only detecting the offset frequency. Further reading on signal analysis after the detector box can be found in Bongham Kim's thesis[5].

The ZaP-HD experiment utilizes a multiple chord interferometry setup in order to locate the pinch. By calculating the density at one axial location, but at multiple impact parameters, the centroid of the pinch can be calculated by looking at where the peak density readings occur. Three chords are used to accomplish this: one through the center of the chamber, and two more above and below the center by approximately 2 centimeters.

Chapter 3
DETERMINING PINCH LOCATION

Characterization of the pinch centroid using several of the diagnostic tools available is still not well understood. Magnetic field probes can give some indication as to centroid location, but they fall short in relating the location to density of the plasma or light emissions from neutral gas. It is important to note, that none of these diagnostics directly measure the plasma centroid location. More detailed information on this is provided in the subsequent pages.

3.1 Determining centroid using magnetic field data

3.1.1 Pinches with short wavelengths

The magnetic field probes on the ZaP-HD experiment are designed to measure plasma current in the chamber. For a pinch located on the z-axis, the magnetic field measured at the outer electrode wall is easily calculated using Ampere's Law. However, an off-axis or bent pinch induces Eddy currents in the wall that attempt to maintain the magnetic flux through the wall. For pinches with a short wavelength relative to the chamber size ($\lambda < 5cm$), the following set of equations are valid and the method used to calculate the centroid is accurate.

The total magnetic field measured at the wall is

$$B = B_0 + B_1 + B_2$$

where B_0 is the magnetic field described by Ampere's Law (above), B_1 is the magnetic field from the loop current emanating from the wall, and B_2 is the magnetic field due to Eddy currents, j_2. Modeling Eddy currents proves to be difficult and time consuming, so some simplifying equations and assumptions must be made to explicitly measure the magnetic

field at the wall.

$$B_{1\perp} + B_{2\perp} = 0$$

at the wall

$$B_1 + B_2 = 0$$

for $r > r_{wall}$

For a cylindrical electrode setup, we can assume that

$$B_{2\perp} = -B_{1\perp}$$

$$B_{2\parallel} = B_{1\parallel}$$

Using these assumptions, we can express the total magnetic field inside the electrode without using the Eddy currents.

$$B_{\parallel} = B_{0\parallel} + 2B_{1\parallel}$$

$B_{1\parallel}$ can be calculated using the described perturbations.

Further development of these equations involved measuring magnetic field with a known current displacement as well as simulated displacements. From these developments, total azimuthal magnetic field at the wall can be modeled by

$$B_\theta = \frac{\mu_0 I}{2\pi r_{wall}} \left(\frac{r_{wall}^2 - d^2}{r_{wall}^2 - 2dr_{wall}\cos\theta + d^2}\right) \tag{3.1}$$

In the case where a displacement changes with axial location, the location of the centroid can be modeled with the equations

$$x(z) = A\cos\left(m\pi\frac{z - l_s}{l_0}\right)\cos\left(n\pi\frac{z - l_s}{l_0}\right) \tag{3.2}$$

$$y(z) = A\sin\left(m\pi\frac{z - l_s}{l_0}\right)\cos\left(n\pi\frac{z - l_s}{l_0}\right) \tag{3.3}$$

where A is the maximum radial displacement, l_s is the starting location of the perturbation, l_0 is the axial extent of the perturbation, m is the number of azimuthal cycles, and n is the number of axial oscillations. Although these equations are valid for the described conditions, using them requires knowledge of the pinch everywhere along its axial length. With current diagnostic tools, this is generally not feasible on the ZaP-HD machine.

3.1.2 Pinches with long wavelengths

For pinches with long wavelengths relative to the chamber, ($\lambda \gg 5cm$), equations 3.2 and 3.3 are not valid. Instead of these equations, the pinch is always assumed to have a long wavelength, and the following method is used to determine centroid location.

$$X(t) = 0.5 \times R_{OuterElectrode} \times M_{1_{norm}}(t) \times cos(\phi_{M1}(t) - \frac{\pi}{8}) \tag{3.4}$$

$$Y(t) = 0.5 \times R_{OuterElectrode} \times M_{1_{norm}}(t) \times sin(\phi_{M1}(t) - \frac{\pi}{8}) \tag{3.5}$$

For all centroid locations determined by the magnetic field probes, the data are calculated using the above equations.

3.2 Determining centroid using Kirana

The data from the Kirana fast-framing camera can provide valuable insight as to the shape and size of the pinch, even if it is not directly measuring the plasma. Several images from the Kirana show the neutral light emissions to be fairly off axis, highly curved, or even split into multiple branches. For this paper, only pinches with well defined edges and a single branch have been analyzed.

3.2.1 Straight, on-axis pinches

The Kirana software has the ability to convert each pixel in a frame into data containing the location as well as the light intensity. Users can pull this data from one specific row or column of pixels at a time. The raw intensity data can be converted to a plot of location versus intensity, as shown below. From this plot, the computer code first determines the edges of the pinch. This is done by calculating an intensity cutoff variable, then determining which pixels meet or do not meet the cutoff value. Pixels with an intensity that meet the cutoff value are considered part of the pinch, while the rest are considered outside of the pinch.

Next, the computer determines the center of the pinch. This is simply done by calculating the middle of the two outermost pixel locations of the pinch. It is also important to note that

the center of the pinch is assumed to be in the center of the neutral cloud. To calculate the pinch location in the chamber, the computer code determines where the center of the pinch is in regards to the edge of the viewing windows. As mentioned previously, the windows on the ZaP-HD machine are 5 centimeters tall, meaning that the edge of the windows are 2.5 centimeters off-axis. The code then compares the center of the pinch to the center and edges of the window, to get a location relative to the window. The code makes the assumption that the camera is perpendicular to the window and that any angled offsets are negligible.

Initial results showed that the code was fairly accurate when analyzing straight, on-axis pinches. However, pinches that were off-axis or curved tended to be inaccurate. More details on the findings will be discussed later. To investigate this, the code was edited to analyze one frame at multiple axial locations to see if there was a relationship between the curve and accuracy of visual analysis.

Initial results from a single axial location showed that for straight, on-axis pinches, the visual emissions and plasma centroid were closely aligned. However, this was not the case for off-axis pinches, or pinches with significant bend to them.

3.2.2 Pinches with instabilities

Analysis of the pinch wavelength was also included to see if the wavelength had any bearing on the accuracy of the code. The rationale behind this is that if a pinch has a short enough wavelength, the equations used to calculate the centroid may become invalid. To accomplish this, multiple axial locations were analyzed for a single frame, and then a third order polynomial was curve fit to the points. To limit any first order, linear terms from skewing the analysis, the points were rotated so that the first and last point were approximately horizontal. The center of a third order polynomial closely resembles the shape of a sine wave, which has a known wavelength that is proportional to the maximum curvature. This means that the maximum curvature of the curve fitted polynomial can be used to approximate the wavelength of its center. The curvature vector, K, for a function, $f(x)$, can be calculated

using the equation

$$K = \frac{\left|\frac{d^2 f}{dx^2}\right|}{[1 + (\frac{df}{dx})^2]^{3/2}}$$

For a sine wave of the form $A \sin cx$, we see that $K_{max} = Ac^2$, where A is the amplitude and c is the frequency. From here, we will be attempting to fit a sine wave onto the small portion of the third order polynomial over which we have plotted. We cannot directly calculate the amplitude and frequency of the sine wave, so we instead calculate K_{max} from the third order polynomial. The amplitude is calculated simply by taking the difference between the highest and lowest points that we plotted, and dividing them by 2. From here, we can calculate the frequency of the sine wave. The wavelength of a sine wave is given by

$$\lambda = \frac{2\pi}{c}$$

In this case, our wavelength had a units of pixels. Similar to the method used to convert centroid pixel locations to centimeters, the wavelength was compared to the size of the viewing window and converted into centimeters. The average curvature over all the axial data points was also calculated to see if there was any correlation as well. Although this wavelength calculation was originally implemented to study atypical pinch shapes, it will be implemented into the analysis for all pinches in this paper.

3.3 Determining centroid using interferometry

As mentioned previously, maximum electron density values have been determined from past interferometry experiments at approximately $10^{23} m^{-3}$. Using this information, we can plot the time resolved density traces onto a surface, and analyze the locations of highest densities. It is assumed that the center of the pinch has the highest density values and the density drops off with radial distance, up to approximately 5mm (reference Increasing plasma parameters paper). The centroid location is determined using all three chord density readings. This is done by fitting a Cauchy-Lorentz probability distribution function to the three chords at every data point. A simple root mean squared equation is used as the objective function to determine the accuracy of the distribution fit. From there, MATLAB's built in fminsearch function is used to minimize the objective function. In addition, a constraint in the form of

a Heaviside function is put on the centroid location to be between $\pm 1.5cm$. Shown below are the equations used in the curve fitting process.

$$f(\gamma, x, x_0, C) = C\frac{1}{\pi}\left(\frac{\gamma}{(x-x_0)^2+\gamma^2}\right)$$

$$RMS(\gamma, x0, C) = 10^{30} \times H(|x0| - 1.5) + \sqrt{\frac{[f(\gamma,1.5,x_0,C)-n_{e1}]^2+[f(\gamma,0,x_0,C)-n_{e2}]^2+[f(\gamma,-1.5,x_0,C)-n_{e3}]^2}{3}}$$

where H is a Heaviside function, C is a scaling factor, γ specifies half the width at half the maximum height, x_0 is the center of the curve, and x is the location on the curve. The heaviside function was included in an attempt to prevent MATLAB from optimizing the curve outside of the bounds of the interferometer chords. MATLAB attempts to minimize the RMS equation by adjusting the three parameters specified. Once it does this, the x_0 term is returned and it is assumed that this is the center of the pinch, according to the interferometer. This method of curve fitting results in MATLAB finding a unique solution. Since there are three unknowns (C, γ, and x_0), and three data points, the current setup results in a determined system. Adding additional chords may cause this curve fitting function to become underdetermined, as it would be trying to fit three variables to more than three data points.

Using this method, we are able to determine location of the pinch centroid, so long as it is within the bounds of the upper and lower scene beams. This gives us a range of 1.5 centimeters above and below the center of the chamber. If the centroid is outside the specified range, then the assumptions used for the equations are violated. In this case, there exists multiple curves that can fit the three data points as well as give a value for $|x_0| > 1.5cm$. To help visualize the data, a three-dimensional plot of chord location vs time vs density is created, along with a surface plot connecting each of the data points together.

Due to size and space constraints of the ZaP-HD lab, one of the chords passes through the vacuum chamber at a slight incidence angle. The incidence angle is small enough that its contribution to the dispersion relation in section 2.2.3 is still negligible. However, the angle will be taken into account when doing final calculations of the density.

Chapter 4

EXPERIMENTAL RESULTS

Here we will present the raw data from the diagnostic suites, as well as the specific settings of the ZaP-HD machine at the time. All of these data points were collected at P15, unless otherwise noted.

4.1 Kirana

Hundreds of pulses were fired over the months in which the data are collected. Below is an excellent example of what a pinch should look like. The edge of the pinch is well defined, the center of the pinch is bright, and the background is dark in comparison. In addition, there are no bright reflections off the back window that would otherwise skew the data.

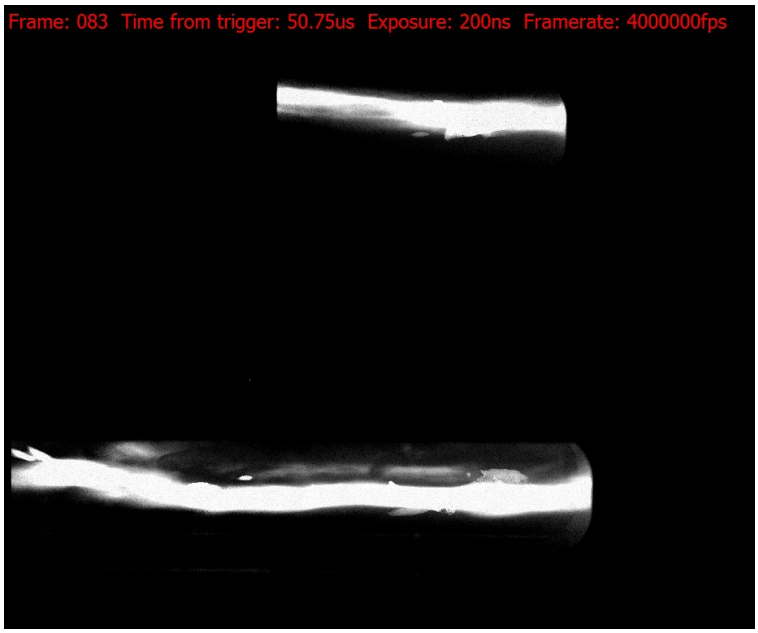

Figure 4.1: This is an ideal example of a Z Pinch. The pinch itself is straight and on-axis, without any major instabilities setting in yet.

In regards to the orientation, the right side of the picture is upstream towards the nosecone and the left side is downstream. The upper portion of the image shows the top-down view of the pinch. The lower portion of this top-down view is in the +x direction and is closer to the camera, while the upper portion is in the -x direction and is farther from the camera. The lower portion of the image shows the side view of the pinch, with the top of it being in the +y direction. See the image below for a diagram of the periscope setup.

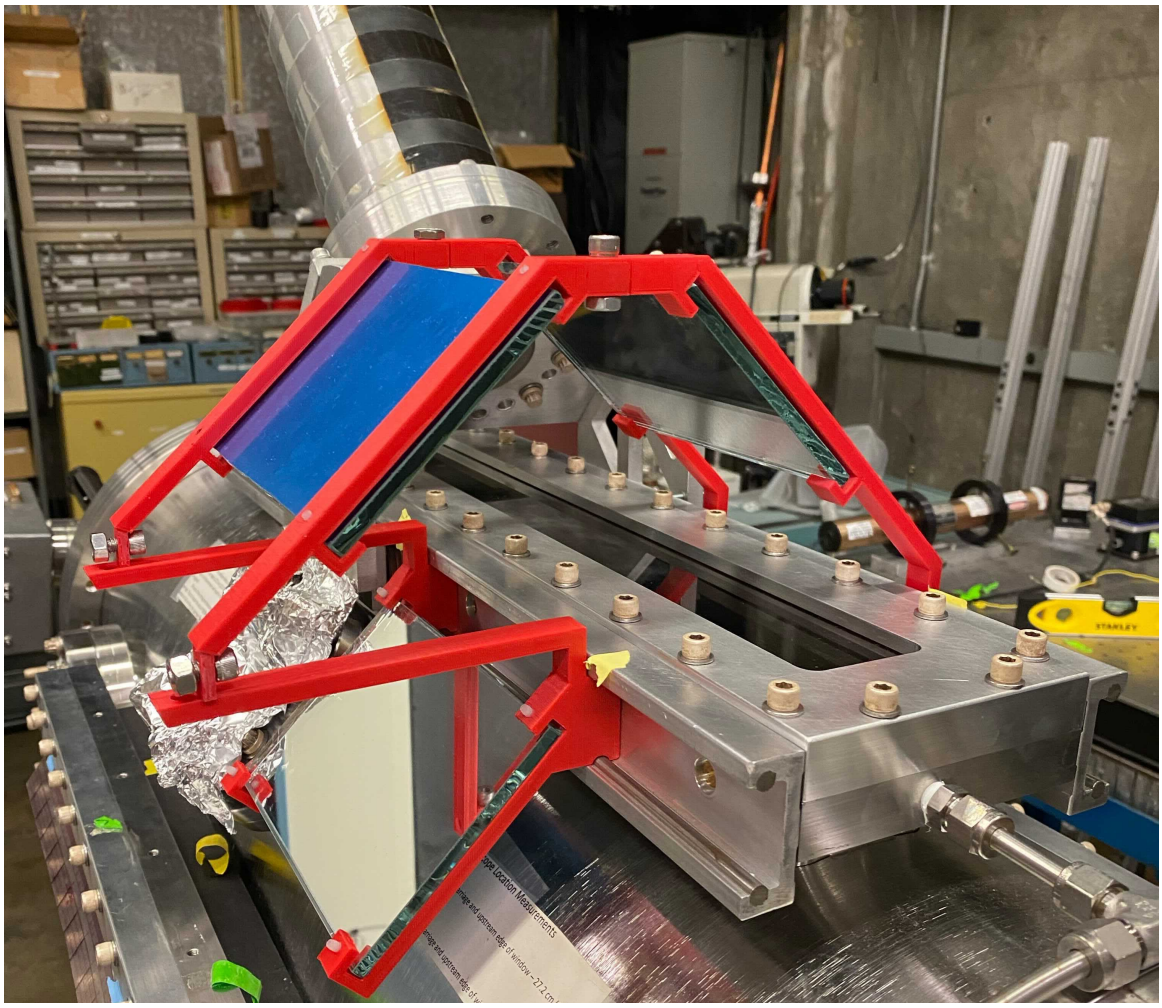

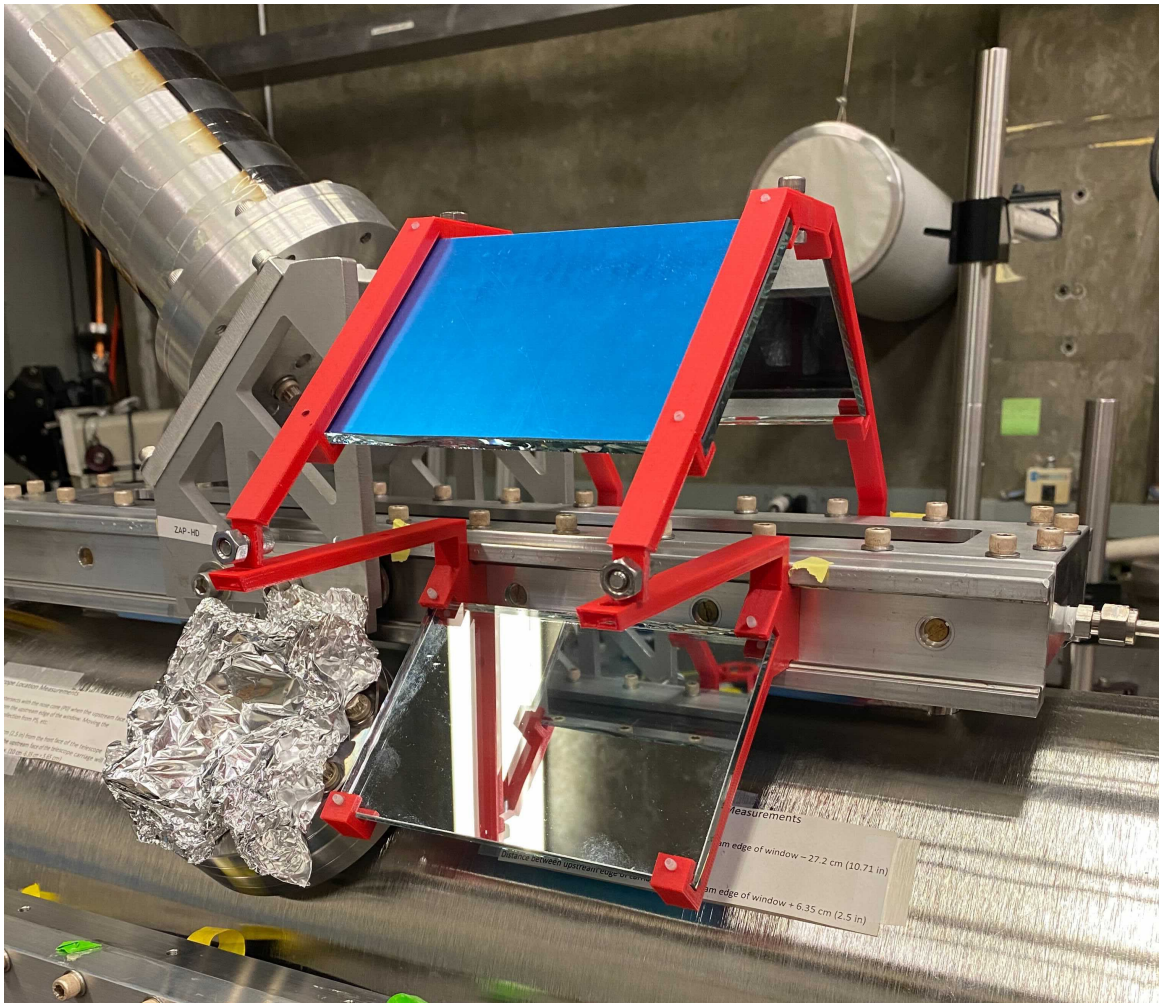

Figure 4.2: Telescope mount on ZaP-HD machine. This allows the Kirana to view both the top and the side of the pinch simultaneously.

Below are several shots taken across multiple days. The pinches themselves showed a wide variety of shapes, brightness, and lengths.

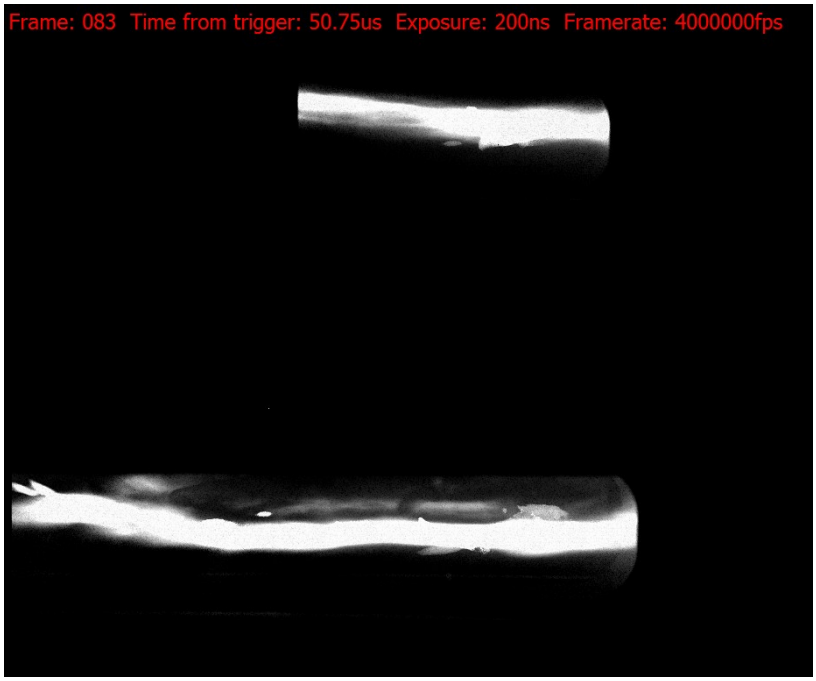

(a) Pulse 210825008

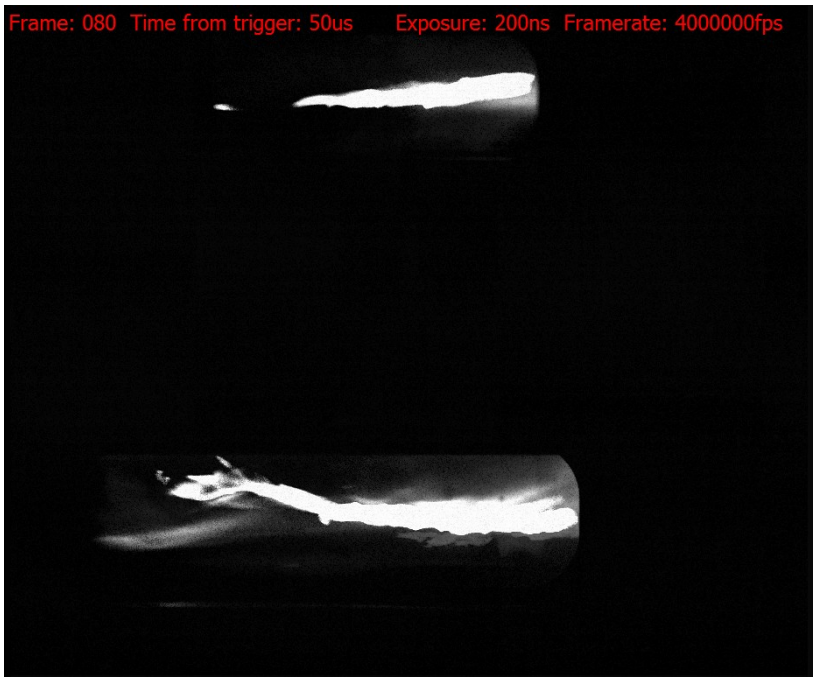

(b) Pulse 210922013

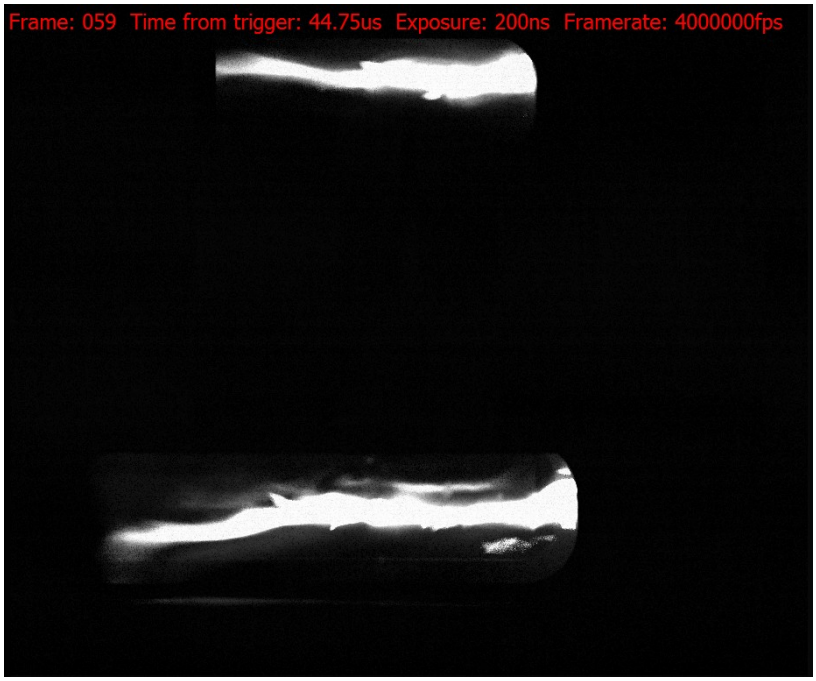

(c) Pulse 210922027

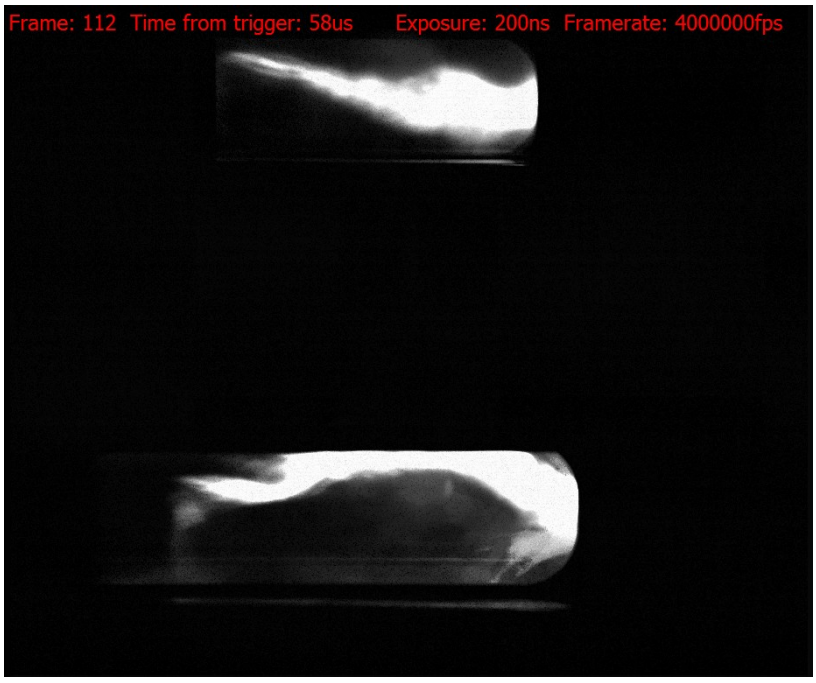

(d) Pulse 210922029

Figure 4.3: These pictures show a set of pinches taken from August 25 and September 22, 2022.

Table 4.1: Table outlining the key parameters used for the first set of pulses

Pulse	$\tau_D(us)$	$P_{gas,I/O}$(Torr)	Voltage V_c/V_a (kV)
210825008	24	4382/3328	5/7
210922013	24	4368/3331	5/7
210922027	24	4368/3331	6/8
210922029	24	4368/3331	6/8

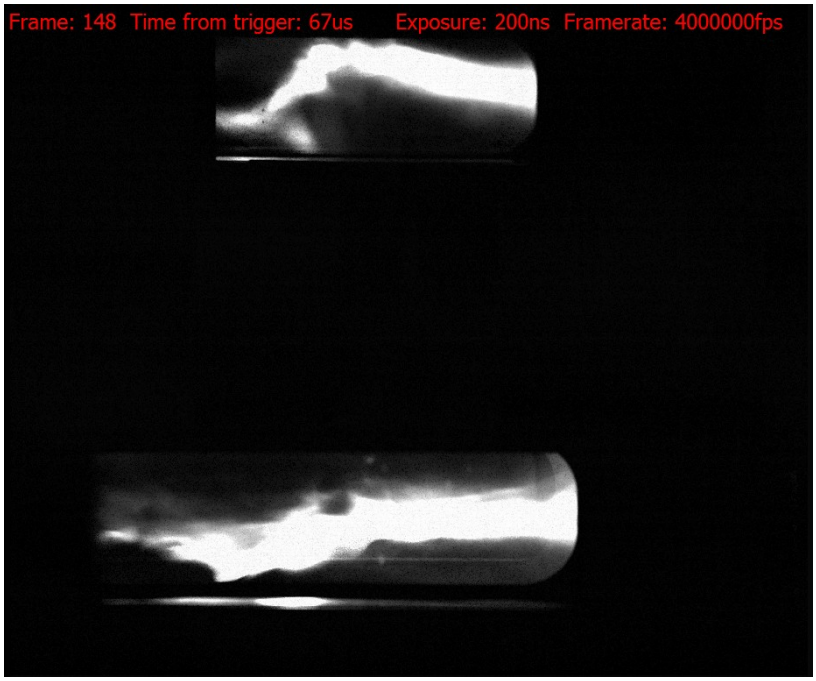

(a) Pulse 210922030

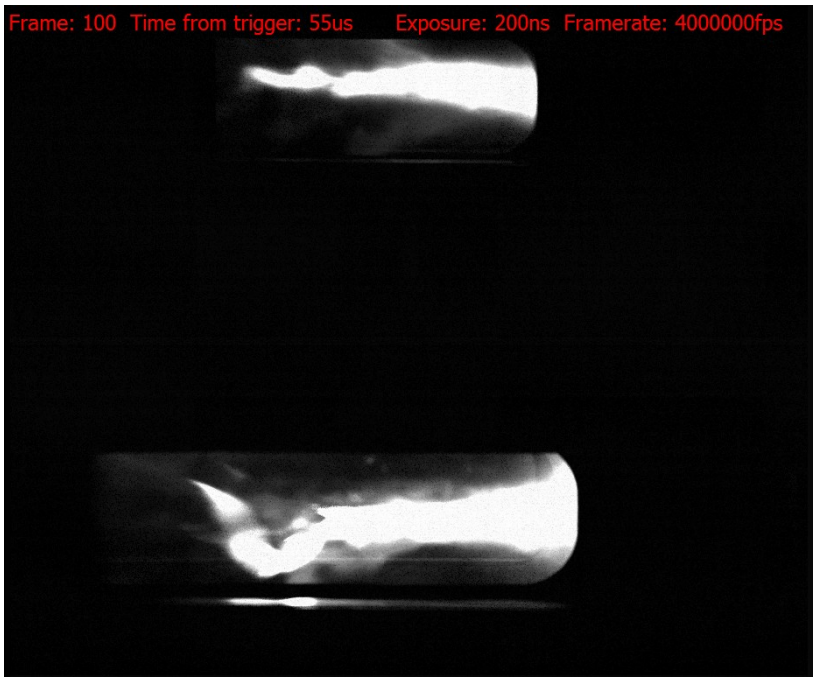

(b) Pulse 210922034

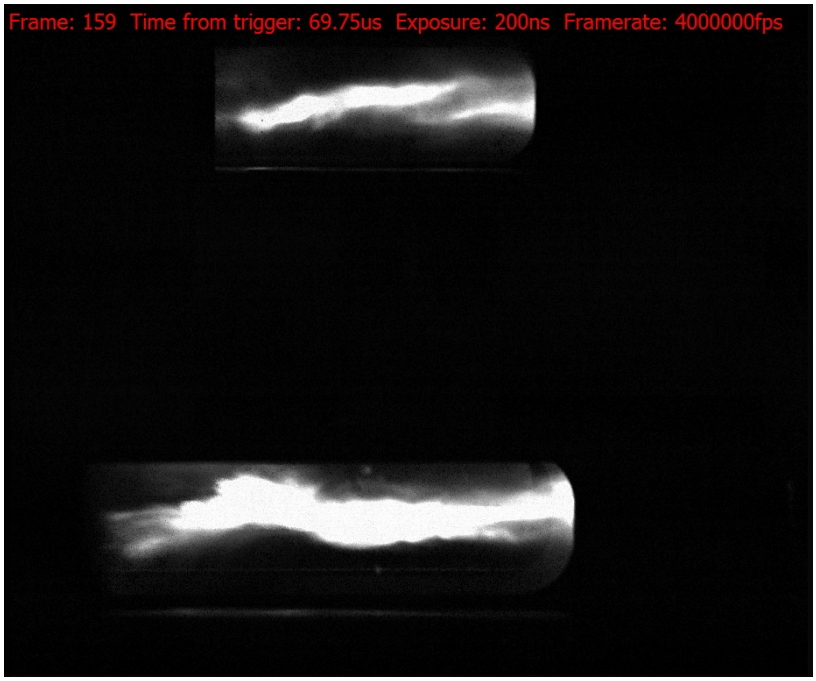

(c) Pulse 210928017

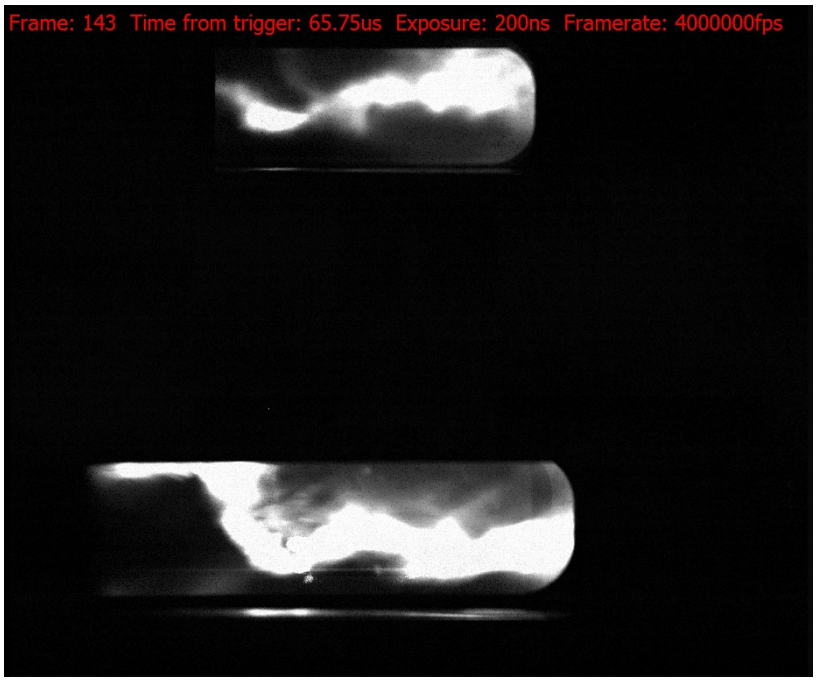

(d) Pulse 210928018

Figure 4.4: These pictures show a set of pinches taken from September 22 and September 28, 2022.

Table 4.2: Table outlining the key parameters used for the second set of pulses

Pulse	$\tau_D(us)$	$P_{gas,I/O}$(Torr)	Voltage V_c/V_a (kV)
210922030	24	4368/3331	6/8
210922034	24	4368/3331	7/9
210928017	24	4377/3332	6/8
210928018	24	4377/3332	6/8

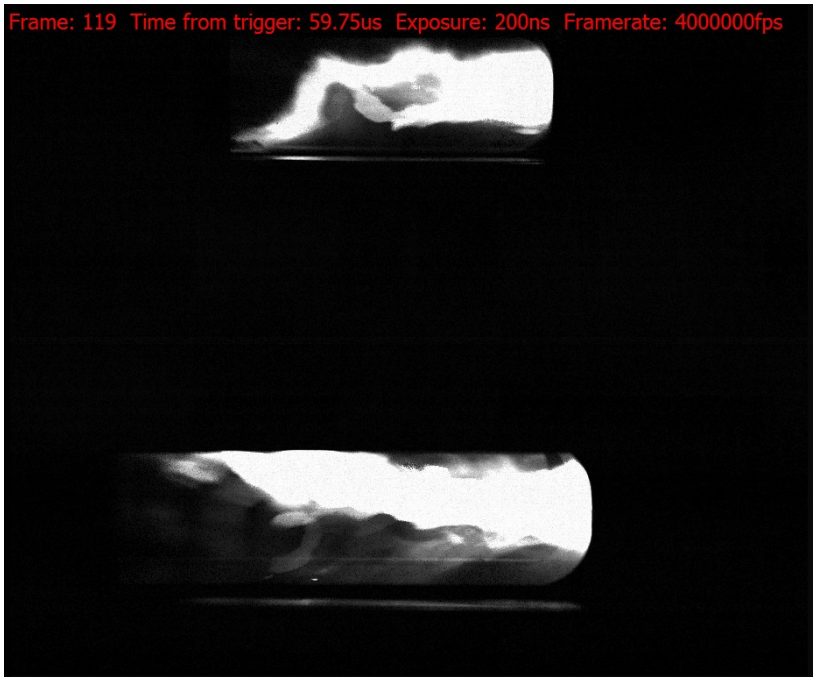

(a) Pulse 211014006

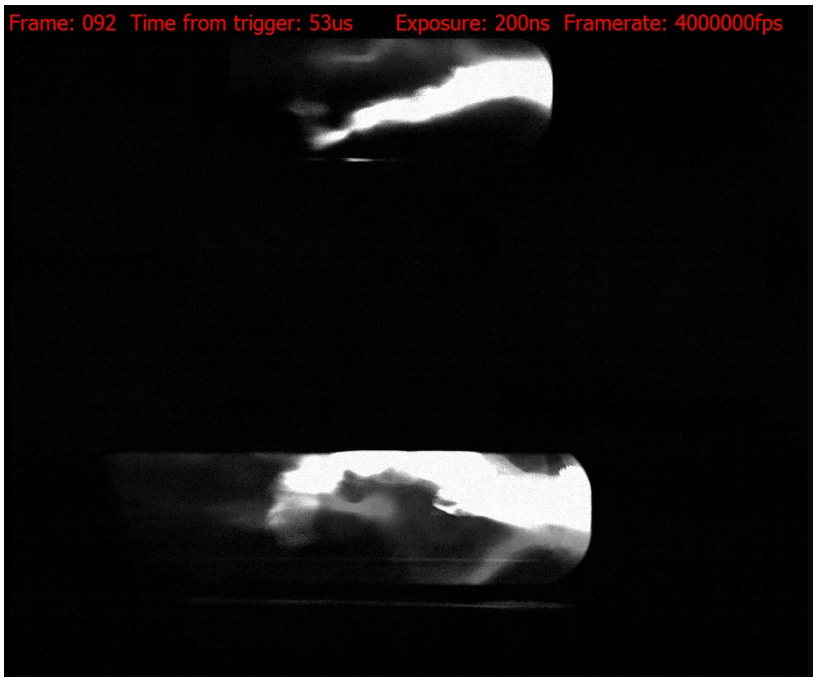

(b) Pulse 211014009

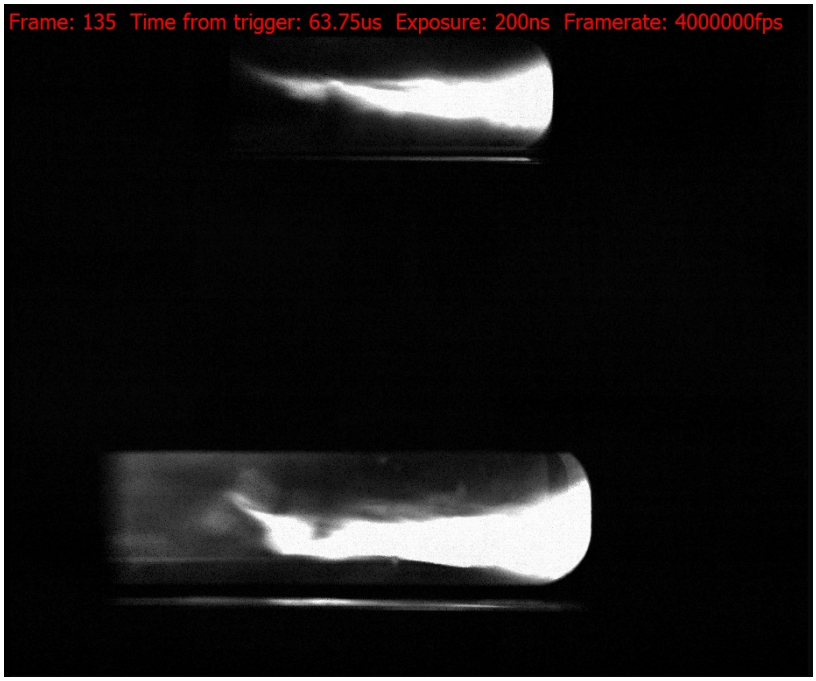

(c) Pulse 211014006

Figure 4.5: These pictures show a set of pinches taken on October 14, 2022

Table 4.3: Table outlining the key parameters used for the third set of pulses

Pulse	$\tau_D(us)$	$P_{gas,I/O}$(Torr)	Voltage V_c/V_a (kV)
211014006	24	4368/3331	6/8
211014009	24	4368/3331	7/9
211014020	24	4377/3332	6/8

At least half of the shots have rough or bumpy edges that can skew the approximated centroid location away from the z-axis. As of now, there is are no known machine parameters to completely eliminate this. On a similar note, some pinches tended to lack well-defined edges. For these pinches, the edges tended to look more like a gradient that could be almost

a centimeter wide. Typically this problem arises if the camera becomes overexposed or the voltage levels delivered to the machine are on the low end (3-5 kV). Another issue commonly experienced by the Kirana diagnostic is reflections from the window opposite the Kirana. Errant reflections coming off the back window would appear in the Kirana video and would show as two separate pinches, or pinches that split off into two. When this happens, the code is unable to determine which pinch is the reflection, and it cannot properly run. This issue can typically be fixed by adjusting the angle at which the camera is recording through the window, but this solution does not always work.

Another set of pulses will also be used to compare the Kirana and interferometry outputs. These differ slightly from the previous pulses in that the Kirana did not need to see the periscope view of the pinch since the interferometer could only resolve centroid location along the y-axis. Shown below is a set of three pulses used for this comparison. Note that pulse 211118018 will be analyzed at two different times.

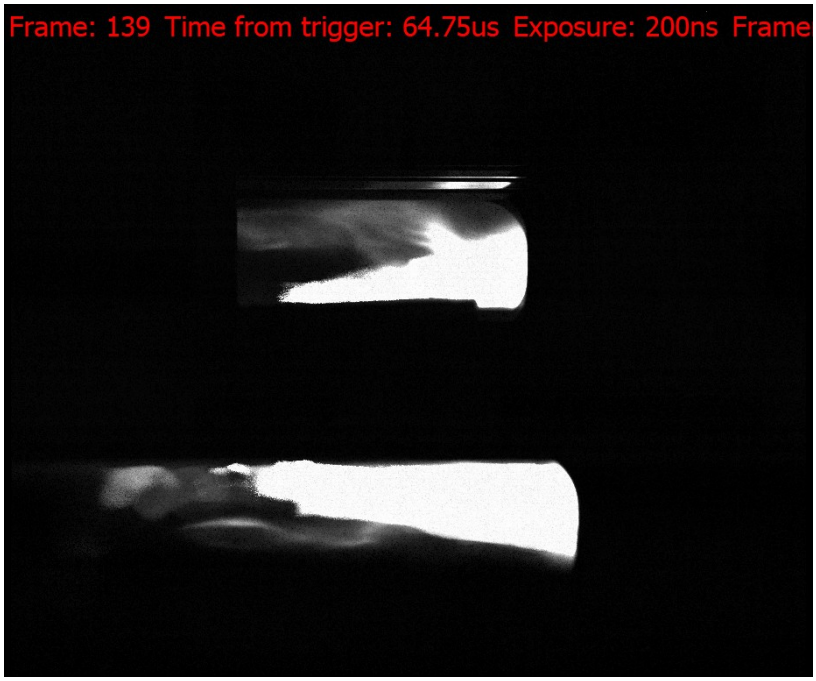

(a) Pulse 211116019

(b) Pulse 211118018 at 36.5 μs

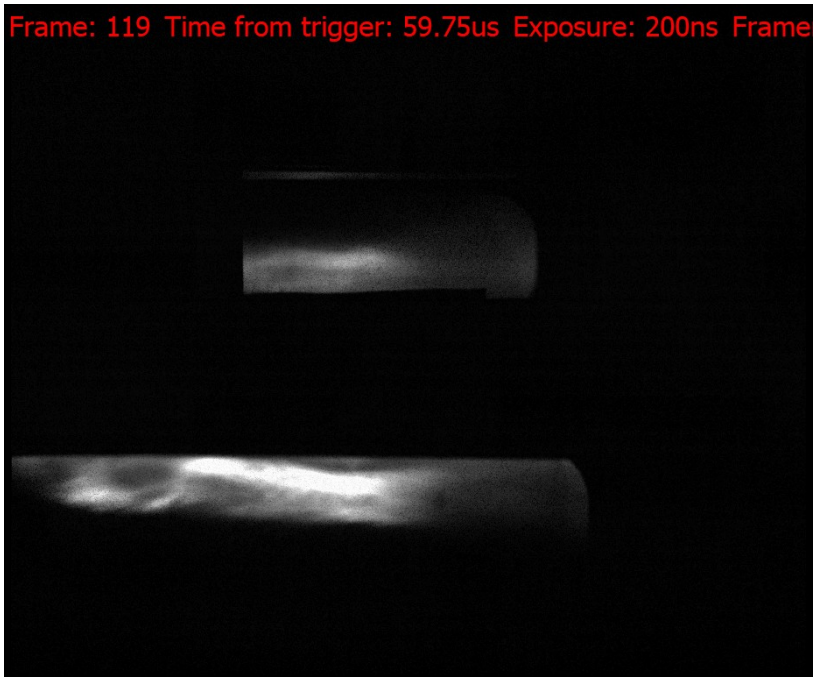

(c) Pulse 211118018 at 59.75 μs

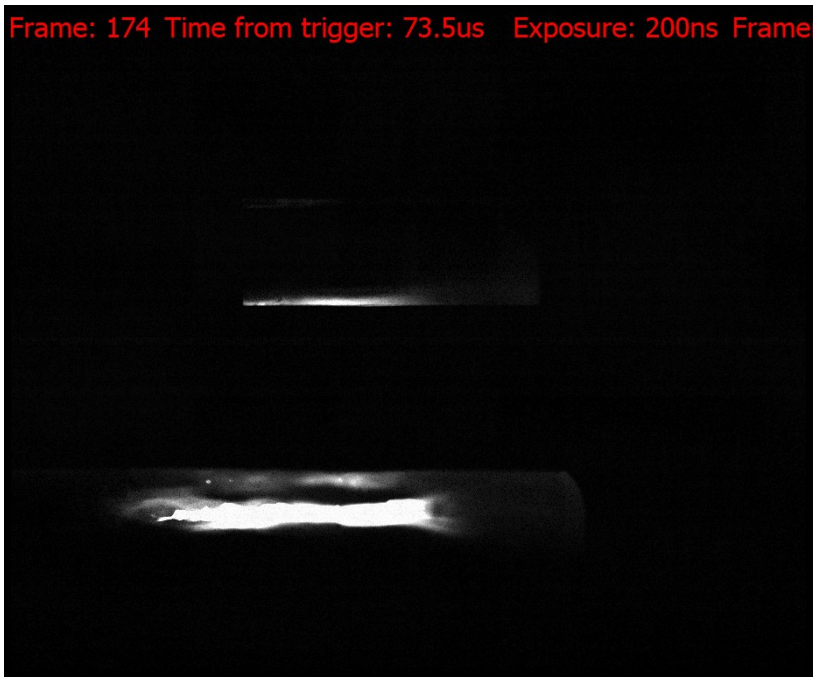

(d) 211209004

Figure 4.6: Pulses that will be used for the comparison between Kirana and interferometry data

Table 4.4: Table outlining the key parameters used for the set of pulses to be used for comparing to the interferometer

Pulse	$\tau_D(us)$	$P_{gas,I/O}$(Torr)	Voltage V_c/V_a (kV)
211116019	24	4330/3324	7/9
211118018	24	4322/3310	5/7
211209004	20	4332/3305	3/5

4.2 Interferometry

The interferometry diagnostics collected excellent data, including the chord that was shot at a small incidence angle relative to the plasma. Typical density values achieved during the pinch were in the range of $10^{22} - 10^{23} cm^{-3}$. Shown below is an example of a single Lissajous figure and the corresponding density data extracted from it, as well as a plot that includes all three traces. Channel 1 (black) indicates data from the top chord at $y = +1.5cm$, channel 2 (blue) indicates the middle chord $y = 0cm$, and channel 3 (cyan) indicates the lower chord $y = -1.5cm$. We see a spike in density once the plasma reaches P15 and the trace continues to remain elevated for the duration of the pinch. Once the pinch has disappeared and the plasma exits the assembly region, the density trace roughly goes back to 0.

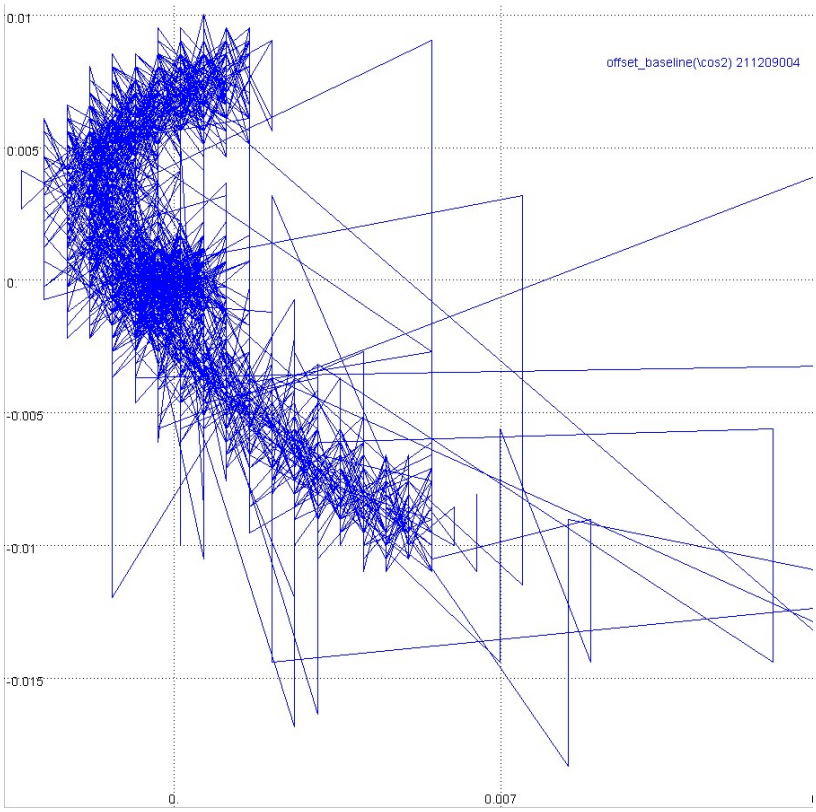

(a) Example Lissajous figure for a single chord for pulse 211209004

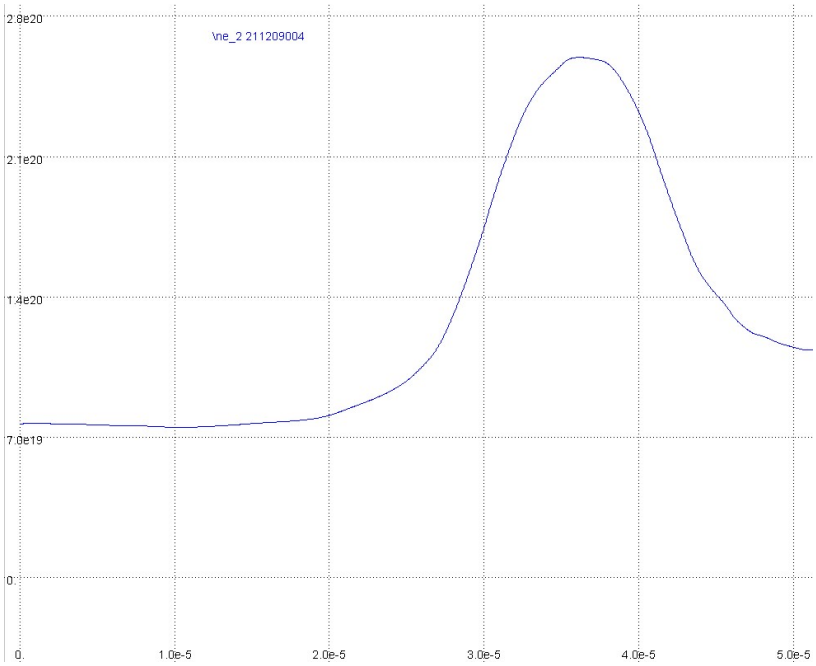

(b) Example density trace for a single chord for pulse 211209004

Figure 4.7: The above pictures show the raw data being output by the interferometry suite.

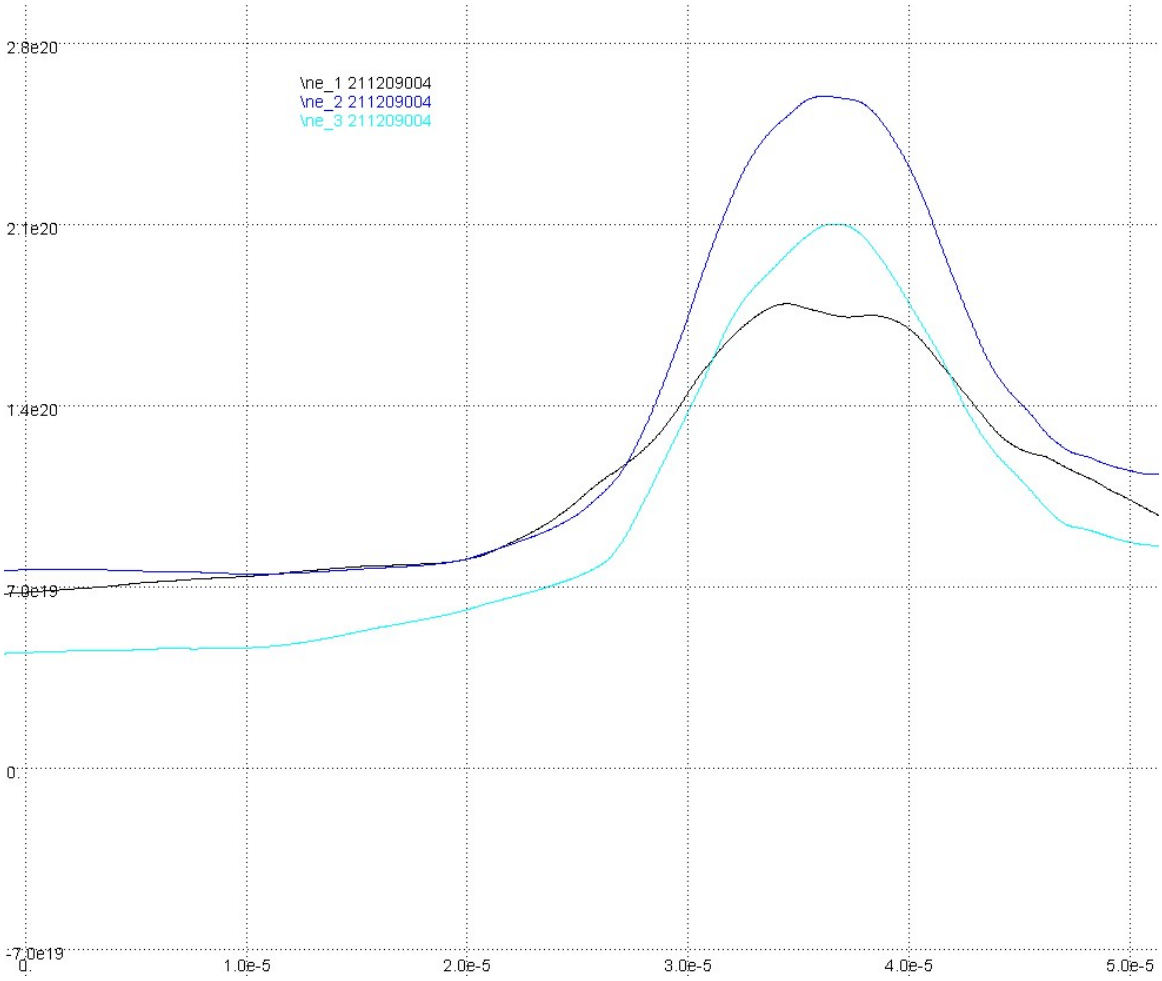

Figure 4.7: Example density trace for all three chords for pulse 211209004

To help better visualize the data, a 3D surface plot was created in MATLAB. The x and y axes are time and location, while the z axis is density. See below for the surface plot of pulse 211209004.

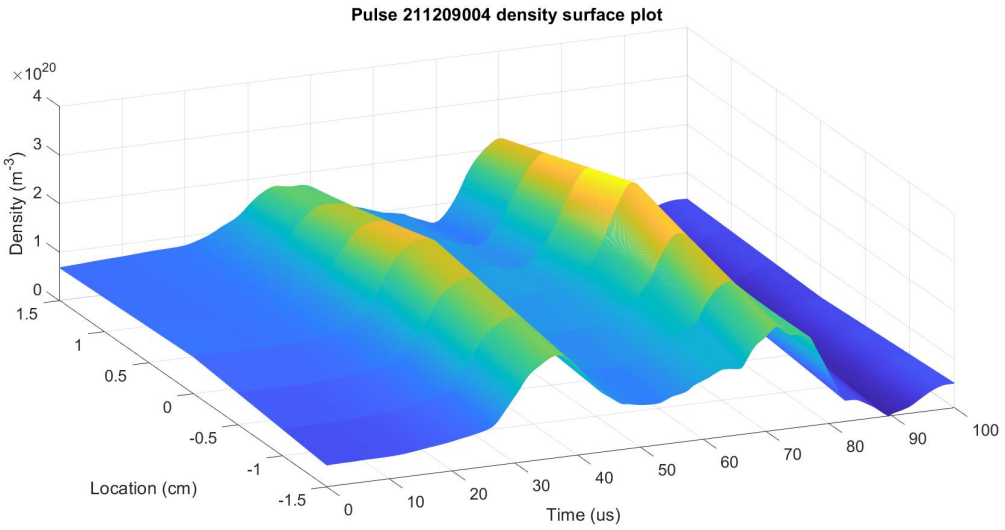

Figure 4.8: Density surface plot populated with density traces from pulse 211209004

As discussed in the previous chapter, a Lorentz distribution function is fitted to the density data. Below is an example of this curve fitting at pulse 211209004 at 50μs.

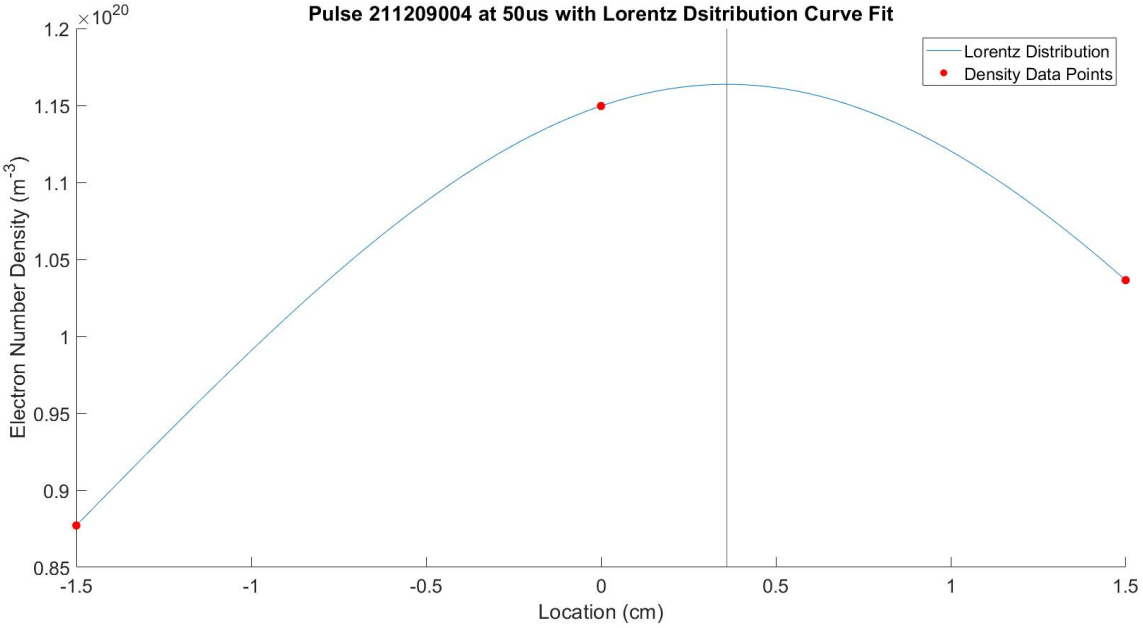

Figure 4.9: This is an example of the Lorentz distribution function being fit to the raw density data points. The black vertical line indicates the center of the distribution function, as well as where the centroid location is inferred to be.

The surface plots for the other pulses in this set are shown below.

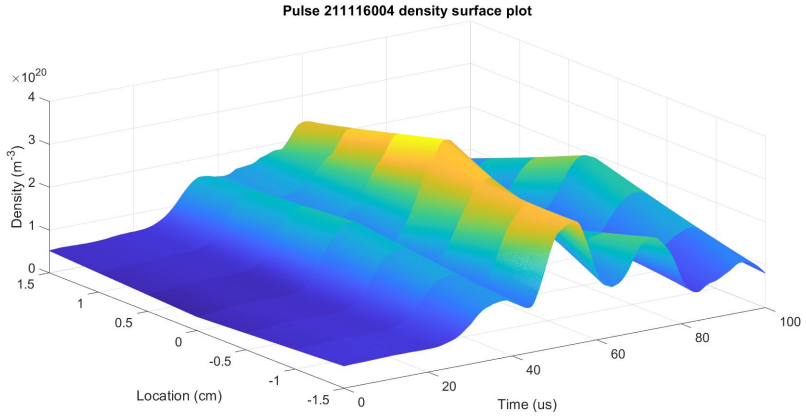

(a) Pulse 211116004

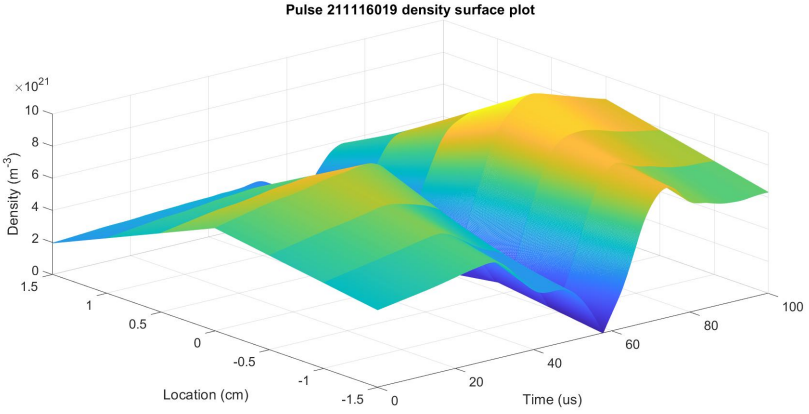

(b) Pulse 211116019

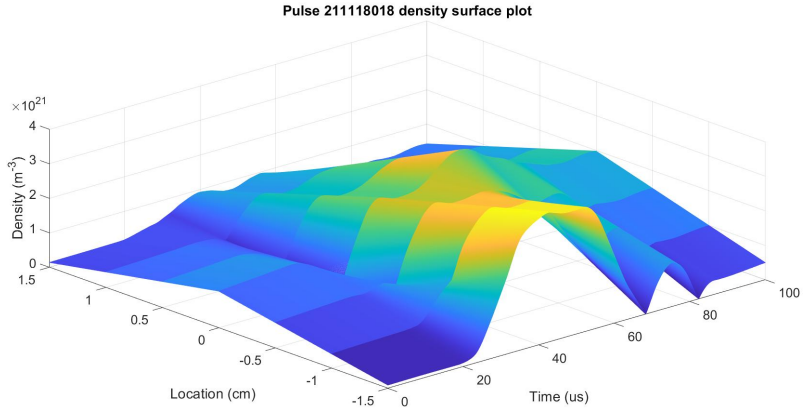

(c) Pulse 211118018

Figure 4.10: The above figures show the surface plots created using the density traces from their respective pulses.

4.3 B Field Probes

The magnetic field diagnostic suite is much more extensive in terms of data points than the Kirana or interferometry setups. Below is an example of raw magnetic field data at one axial location and multiple azimuthal locations.

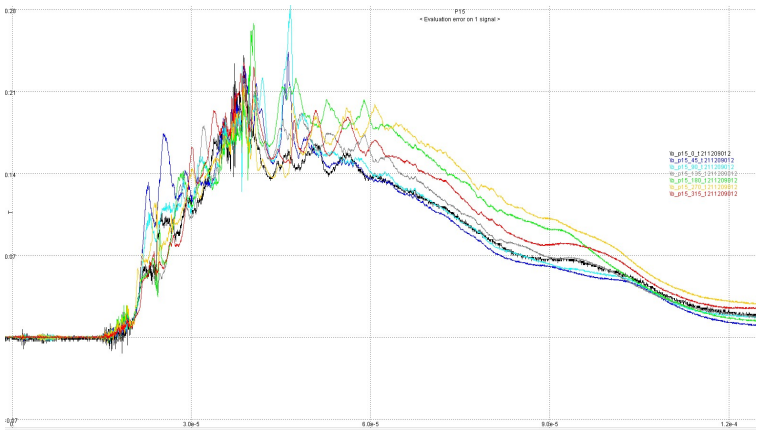

(a) Example Raw B Field Data

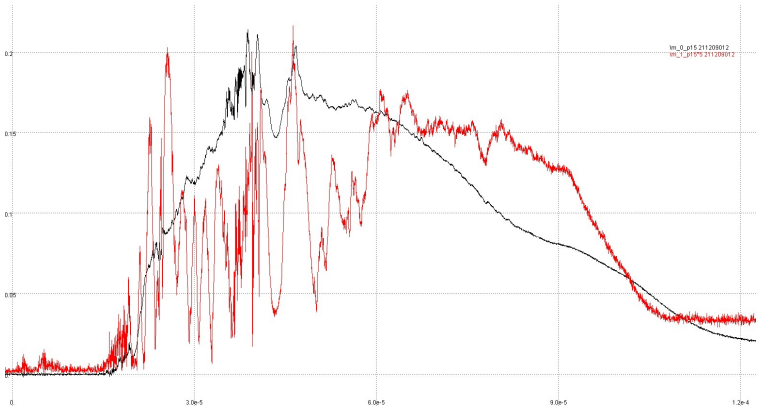

(b) Mode data

Figure 4.11: The above pictures show the magnetic field traces used to calculate the centroid, as described by equations 3.2 and 3.3. Each trace on the top plot is the magnetic field at various azimuthal locations at P15. The second plot shows the $m = 0$ and $m = 1$ mode data, shown in black and red, respectively. The $m = 1$ mode generally describes how off center the pinch is.

Using the raw field data, we extract the $m = 0$ and $m = 1$ mode traces, as seen in 4.11b. From equations 3.2 and 3.3, we can also plot the centroid location of the pinch using magnetic field data. Below is an example of magnetic field centroid location. The red lines indicate the edge of the viewing window, and anything outside of that may be out of sight for the Kirana. The blue lines indicate the boundary of where the pinch is considered in the quiescent region. The cyan and green lines are the centroid locations along the x and y axes, respectively.

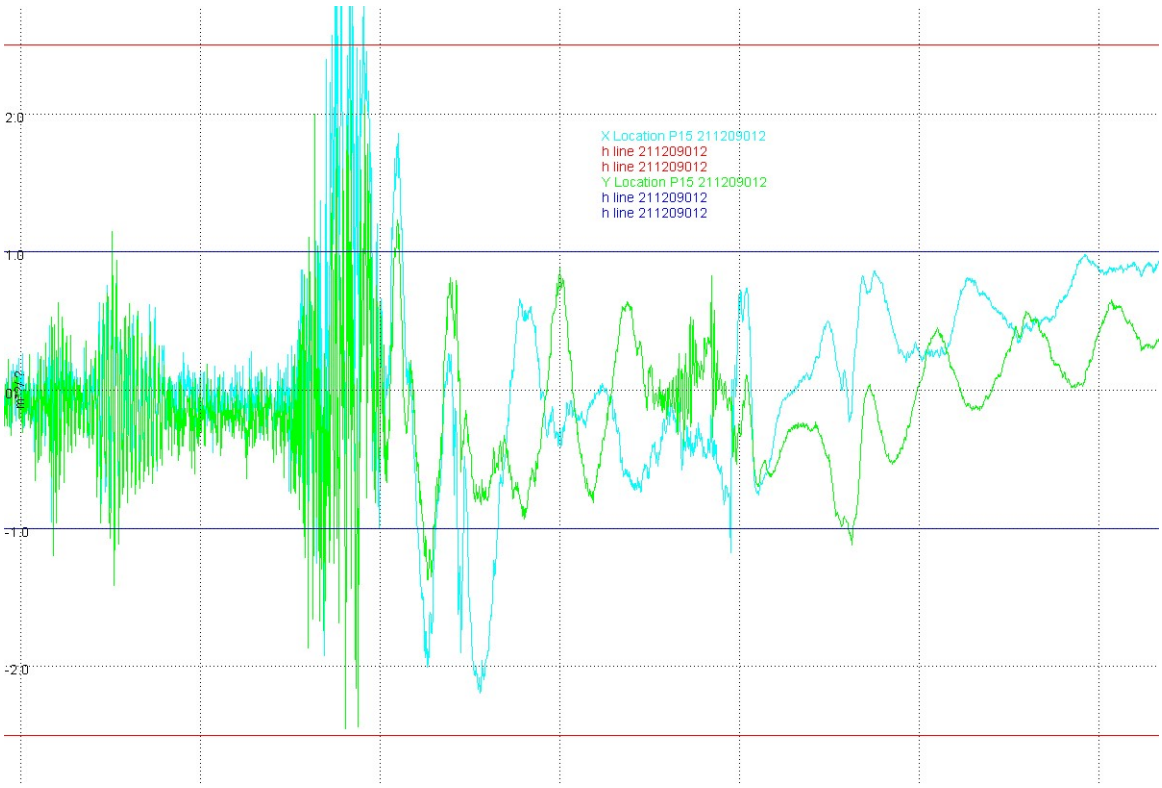

Figure 4.12: An example of magnetic field centroid data for pulse 211209012. The x axis is time (in μs) and the y axis is location (in cm)

Chapter 5

ANALYSIS AND COMPARISON OF DIAGNOSTIC TOOLS IN DETERMINING CENTROID LOCATION

To help with the comparison, this chapter will compare only two diagnostics at a time in each section. At the end, all three diagnostic results will be brought together to examine the relationship between all of them. This chapter will examine any underlying relationships between the diagnostics and will examine the accuracy of them in determining the plasma centroid.

5.1 Comparison of Kirana and B Field Probes

The pinches from the last chapter will be grouped qualitatively by visual appearance. For this section of analysis, three sets of pinches will be analyzed. The first set of pinches presented tended to be straight, on-axis, and well defined around P15. The second set tended to be slightly more unstable or off-axis around P15. The last set showed extreme instabilities and tended to be very off-axis. Below is the first set of pulses.

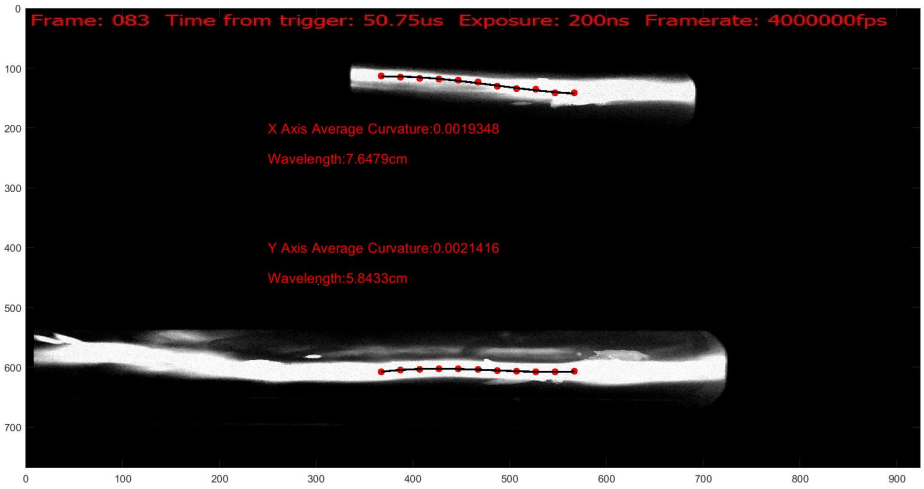

(a) Pulse 210825008

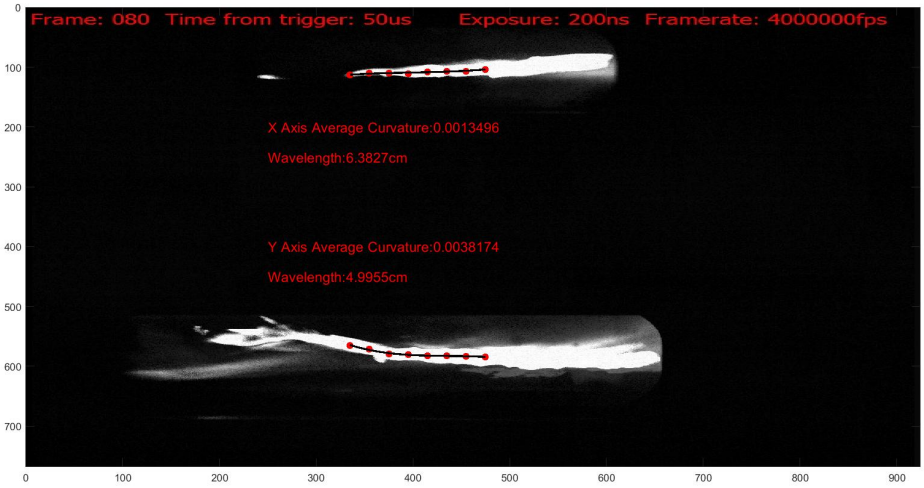

(b) Pulse 210922013

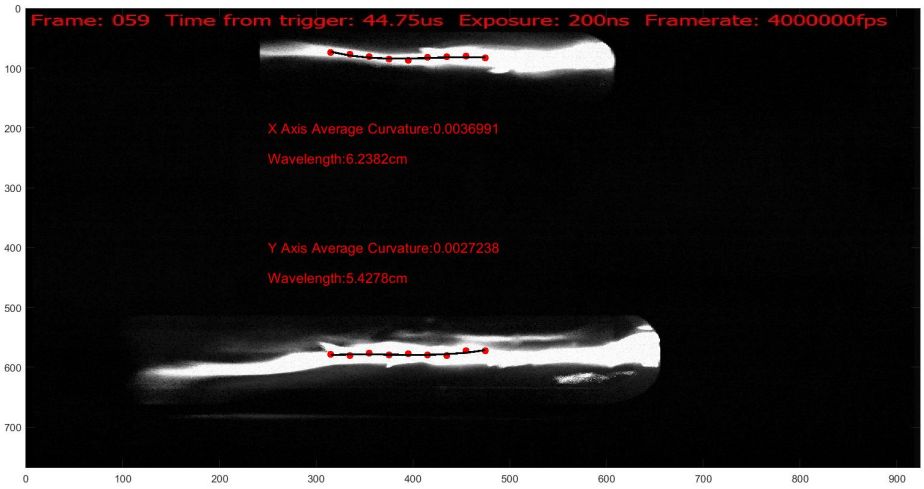

(c) Pulse 210922027

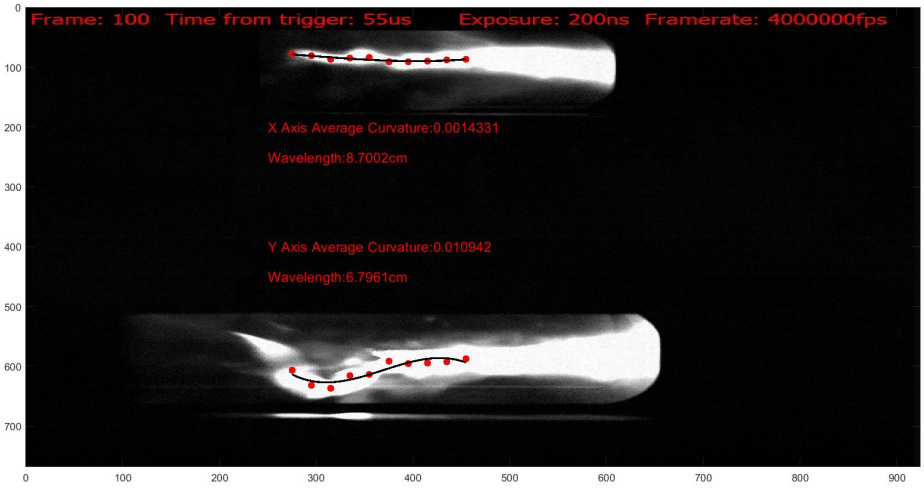

(d) Pulses 210922034

Figure 5.1: First set of pulses with wavelength analysis and centroid analysis at multiple axial locations.

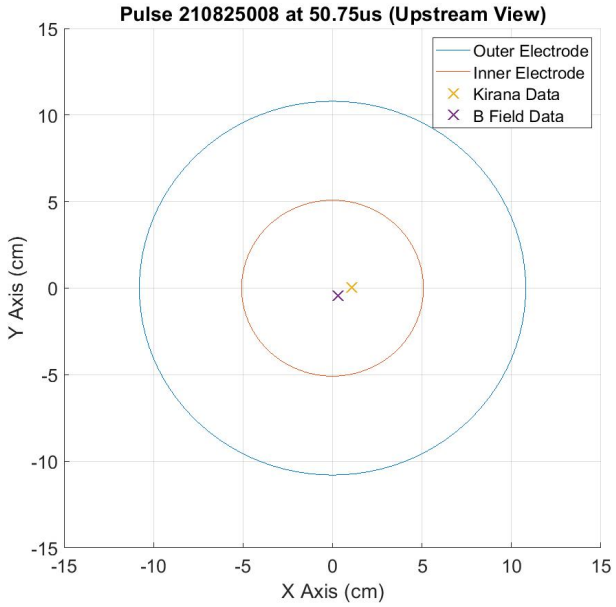

(a) Pulse 210825008

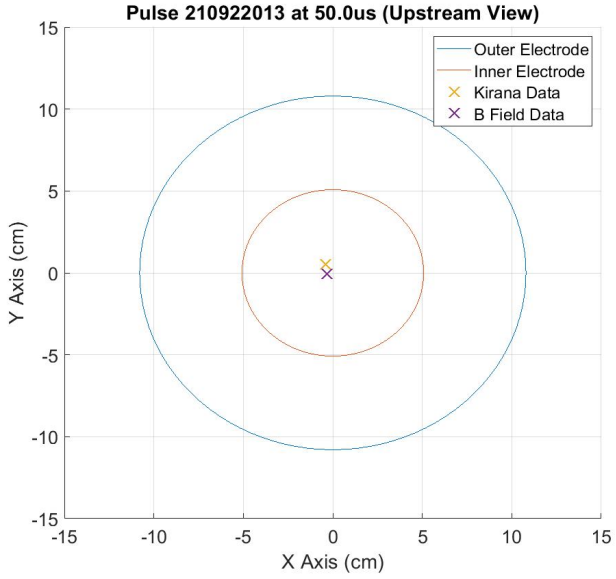

(b) Pulse 210922013

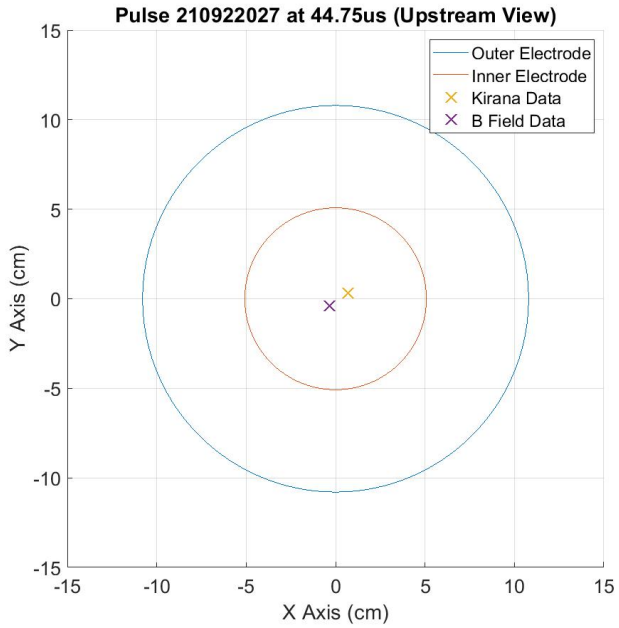

(c) Pulse 210922027

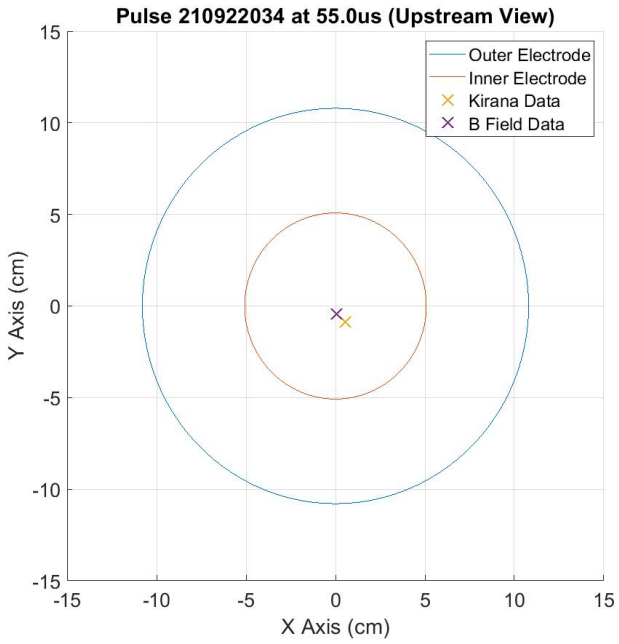

(d) Pulse 210922034

Figure 5.2: The above pictures show the comparison between the Kirana and magnetic field probe centroid data at P15 for the first set of pulses.

The numerical outputs for centroid location have been tabulated below. The distance of the centroid from the z-axis for each method has also been included.

Table 5.1: This table outlines the centroid locations calculated using both the Kirana and the magnetic field probes from the first set of pulses.

Pulse	Kirana	B Field Probes	Δ_{Kz}	Δ_{Bz}	Δ_{KB}
210825008	(1.09,0.04)	(0.31,-0.43)	1.09	0.53	0.91
210922013	(-0.41,0.51)	(-0.33,-0.06)	0.65	0.34	0.58
210922027	(0.68,0.33)	(-0.33,-0.40)	0.76	0.52	1.25
210922034	(0.56,-0.87)	(0.05,-0.44)	1.03	0.44	0.67

Δ_{Kz} is the distance from the z axis to the Kirana centroid data point, Δ_{Bz} is the distance from the z axis to the magnetic field centroid data point, and Δ_{KB} is the distance from the Kirana to the magnetic field centroid data points, all in centimeters.

These initial data show that the Kirana tended to overestimate the centroid distance from the z-axis. Both diagnostics were reading within one pinch radius of each other, with the exception of pulse 210922027. Pulse 210825008 also shows an interesting data trend. Although it looks to be the straightest and closest pinch to the center, it actually had one of the largest deviations from the magnetic field for this set of pulses. This set of pulses had an average Δ_{KB} of 0.85 cm.

The next pulses are either slightly bent or off-axis around P15.

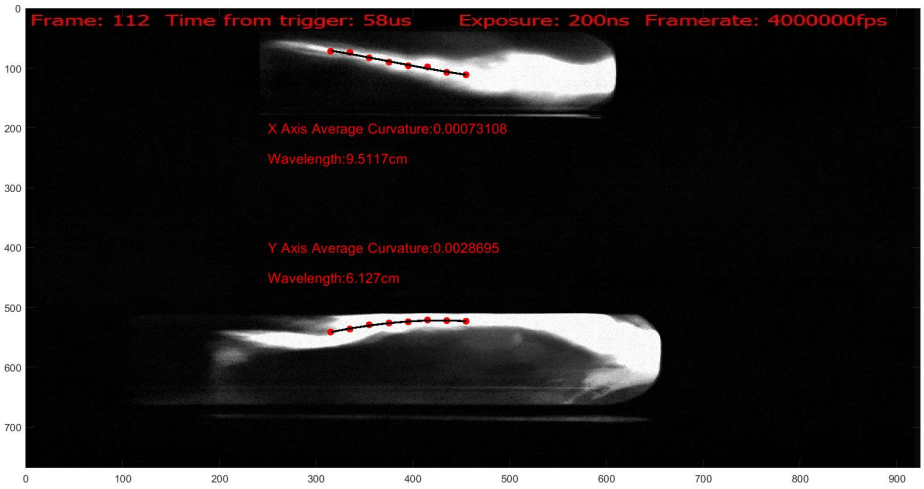

(a) Pulse 210922029

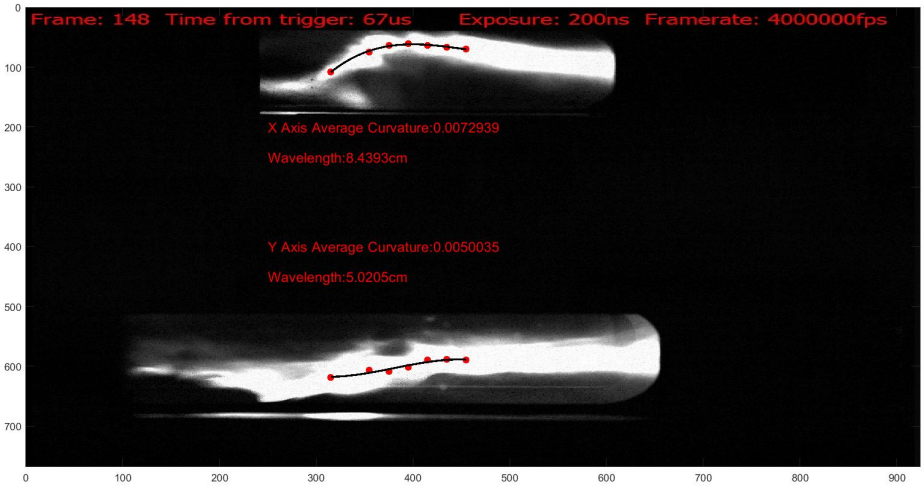

(b) Pulse 210922030

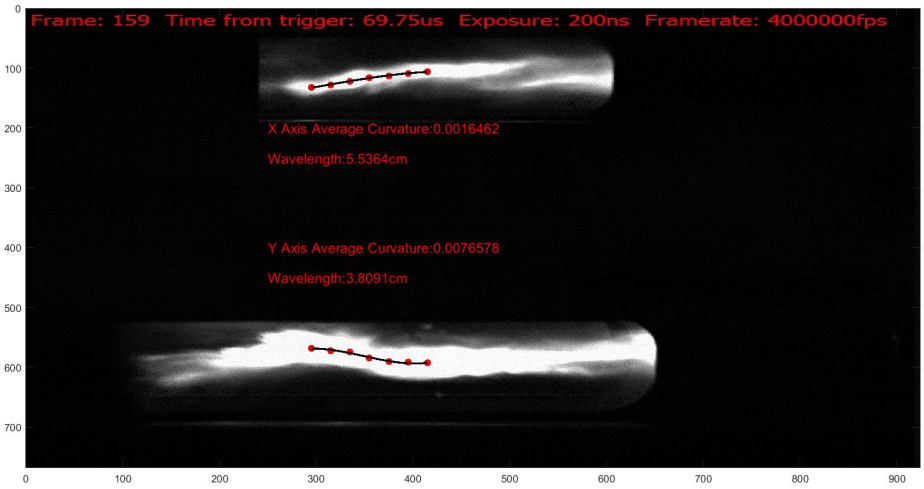

(c) Pulse 210928017

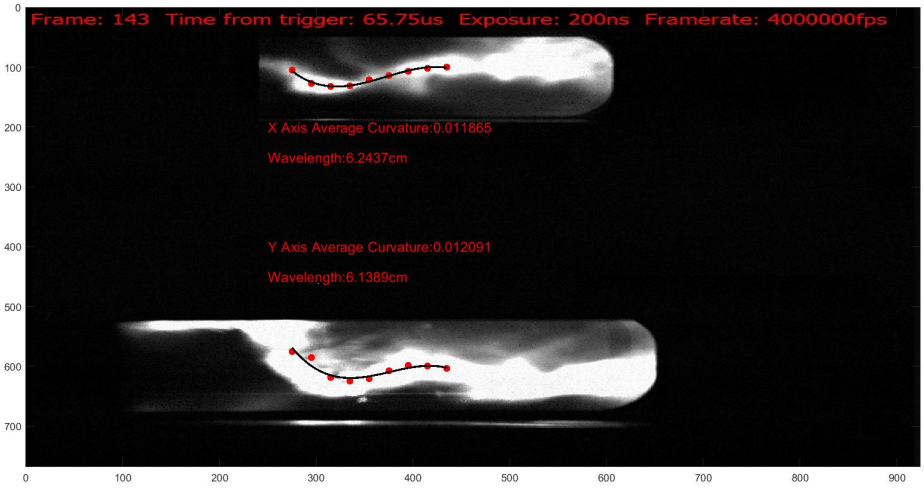

(d) Pulse 210928018

Figure 5.3: Second set of pulses with wavelength analysis and centroid analysis at multiple axial locations.

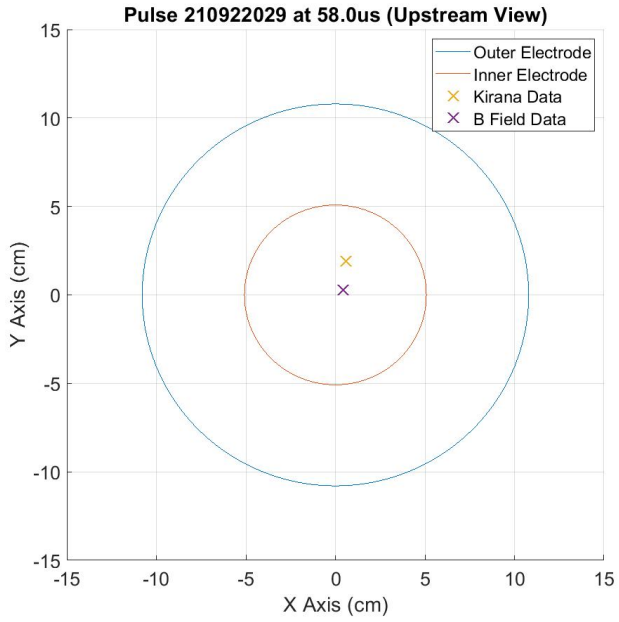

(a) Pulse 210922029

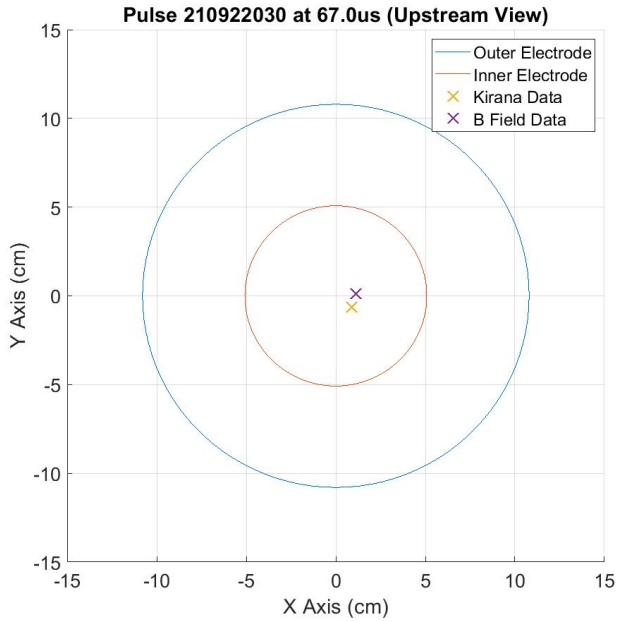

(b) Pulse 210922030

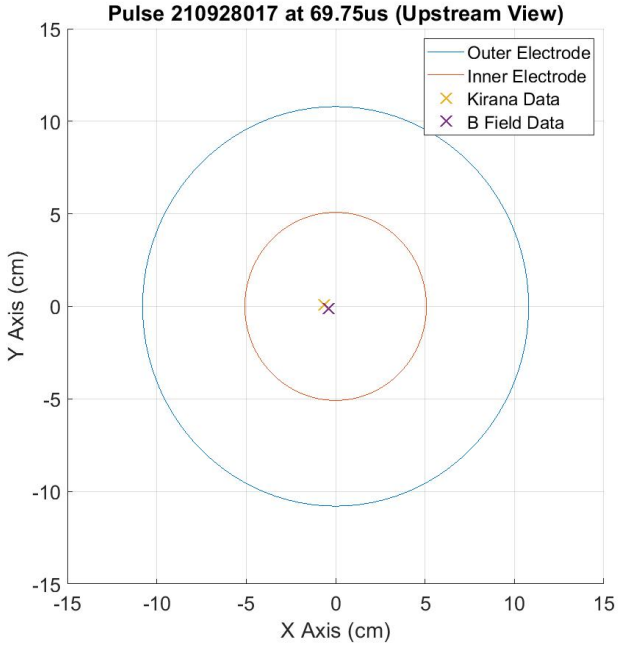

(c) Pulse 210928017

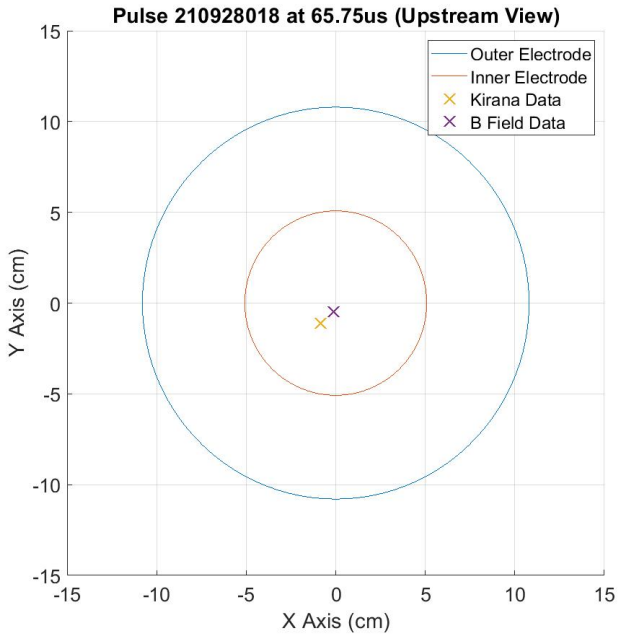

(d) Pulse 210928018

Figure 5.4: The above pictures show the comparison between the Kirana and magnetic field probe centroid data at P15 for the second set of pulses.

Table 5.2: This table outlines the centroid locations calculated using both the Kirana and the magnetic field probes from the second set of pulses.

Pulse	Kirana	B Field Probes	Δ_{Kz}	Δ_{Bz}	Δ_{KB}
210922029	(0.58,1.89)	(0.44,0.27)	1.98	0.52	1.63
210922030	(0.90,-0.64)	(1.11,0.14)	1.10	1.12	0.81
210928017	(-0.64,0.08)	(-0.37,-0.14)	0.64	0.40	0.34
210928018	(-0.85,-1.10)	(-0.13,-0.49)	1.39	0.51	0.94

With the exception of pulse 210922029, the Kirana and B Field probes still read within approximately one pinch radius of each other. Pulse 210928017 had an interesting result compared to the other pulses in this set. Although it was angled relative to the z-axis, the pulse was still straight and well defined. Figure 5.4c shows that the Kirana and B Field probes agree very closely on the location of the centroid. Pulse 210922030 looks similar to 210928017, but the data deviated from each other by approximately half a centimeter in the y direction. This may be in part due to the 'wispy' edge of the pinch around P15 for pulse 210922030. This rough or wispy edge of the pinch was extremely common in the Kirana video and often affected the analysis. This set of pulses had an average Δ_{KB} of 0.93 cm.

The Kirana also captured several pinches with severe instabilities or pinches with atypical visual qualities. The Kirana and magnetic field probes varied much more than in the previous sets of shots analyzed.

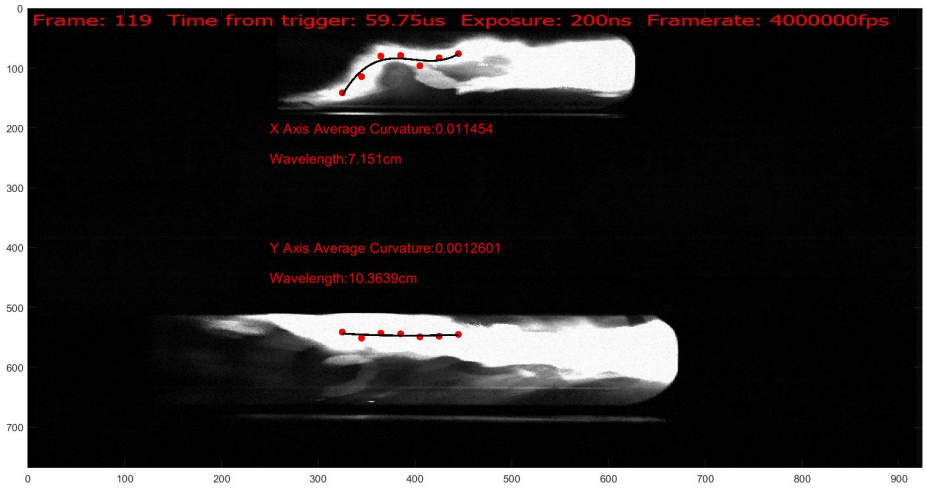

(a) Pulse 211014006

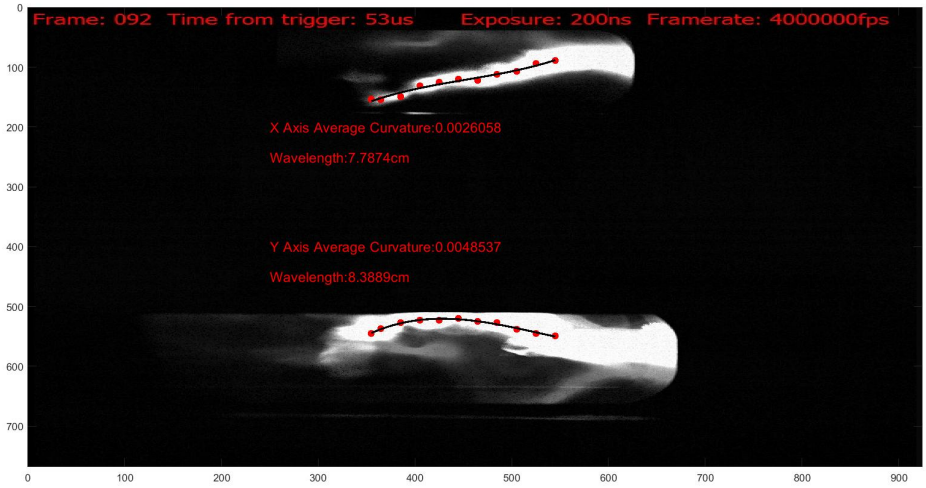

(b) Pulse 211014009

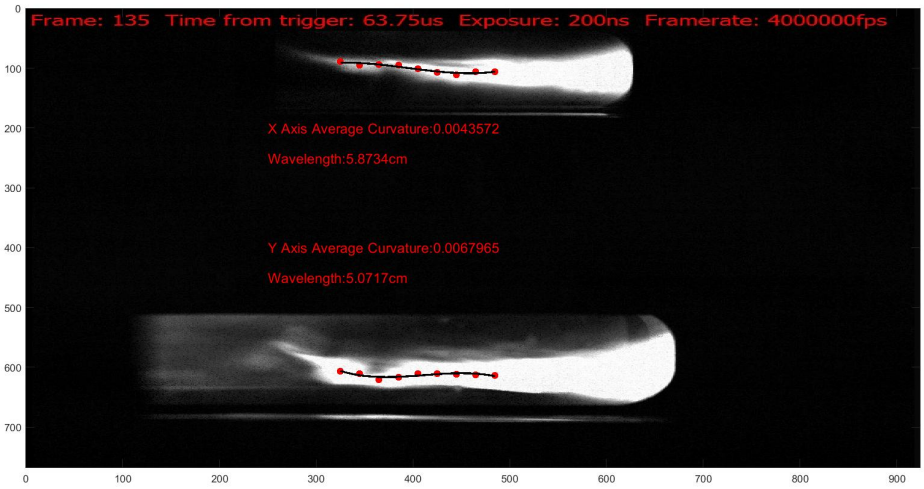

(c) Pulse 211014020

Figure 5.5: Third set of pulses with wavelength analysis and centroid analysis at multiple axial locations.

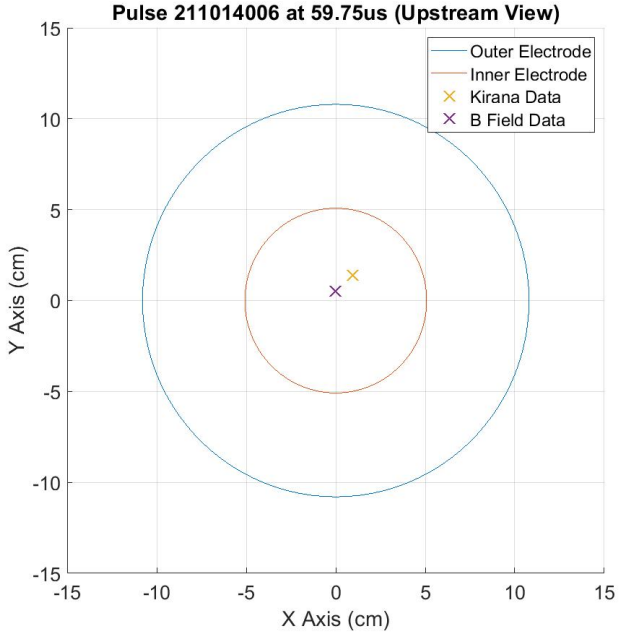

(a) Pulse 211014006

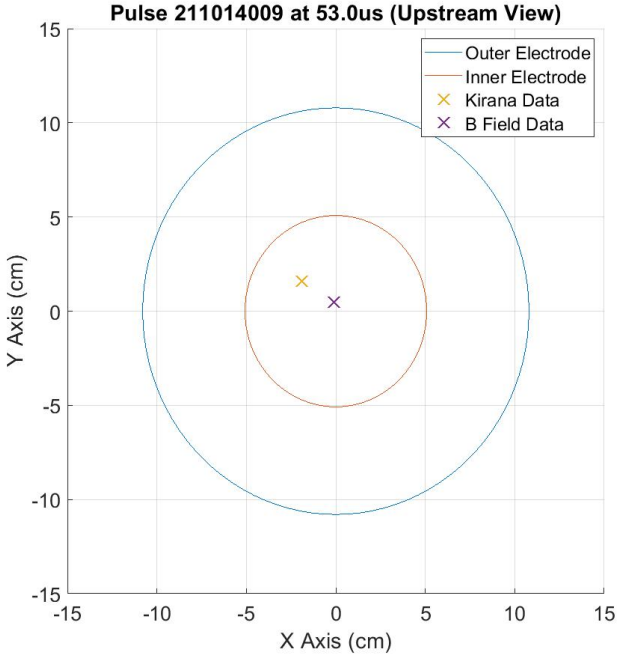

(b) Pulse 211014009

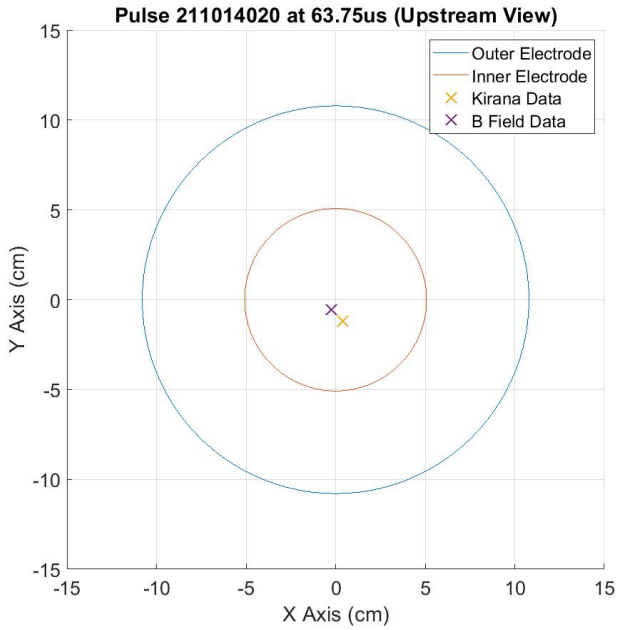

(c) Pulse 211014020

Figure 5.6: The above pictures show the comparison between the Kirana and magnetic field probe centroid data at P15 for the third set of pulses.

Table 5.3: This table outlines the centroid locations calculated using both the Kirana and the magnetic field probes from the third set of pulses.

Pulse	Kirana	B Field Probes	Δ_{Kz}	Δ_{Bz}	Δ_{KB}
211014006	(0.93,1.40)	(-0.04,0.53)	1.68	0.53	1.30
211014009	(-1.89,1.60)	(-0.09,0.47)	2.48	0.48	2.13
211014020	(0.38,-1.18)	(-0.23,-0.56)	1.24	0.61	0.87

With the exception of pulse 211014020, the pulse centroids in this set varied more than one pinch radius between the Kirana and magnetic field probes. Pulse 211014009 actually

varied by more than two pinch radii, which was one of the most drastic differences seen between all of the pulses considered for this paper. This set of pulses had an average Δ_{KB} of 1.43 cm.

Between all of these pulses, multiple trends appeared. One glaring issue between the results of these two diagnostics is that the Kirana almost always overestimated the displacement from the z-axis. For most shots, the magnetic probes showed that the pinch centroid remained within 1 centimeter of the z-axis for almost the entire pulse. However, the Kirana showed that it would deviate much more than the 1 centimeter. Although the Kirana overestimated the distance from the center, it still agreed within a pinch radius for any straight pinches, or pinches with minor instabilities. For pinches with major instabilities, the two diagnostics disagree. As stated in chapter 3, the code used to determine the centroid data relies on the assumption that the pinch is straight and does not contain instabilities. As instabilities grow at the end of the quiescent period, those assumptions are violated and the magnetic field probes may have trouble accurately determining centroid location.

Simply based on a qualitative, visual analysis, the initial equations used to calculate wavelength may be erroneous. Pulses such as 210825008, which were extremely straight and long, showed shorter wavelengths than something such as pulse 210928018, which had clear curvature and a short wavelength. This is most likely a result of including the amplitude in the wavelength calculations. Most straight pinches had low amplitude waves, and this tended to skew the results because of the equations we used. If this method of determining wavelength is continued, it may be beneficial to attempt to resolve any amplitude issues that may arise. At this time, there is low confidence in saying whether there is a correlation between magnetic field probe centroid data and wavelength, or not.

5.2 Comparison of Kirana and IF

Comparison between the Kirana and interferometer diagnostics is limited due to the fact that the sampling rate on the Kirana is much lower than the interferometer. This section will only attempt to compare outputs along the y-axis for single frames during the pulses. In addition, the placement of the Kirana is partially obscured by the interferometry mirrors. To get a better view, the Kirana needed to be angled slightly, which skewed its results.

Below are the centroid location plots from the interferometry data.

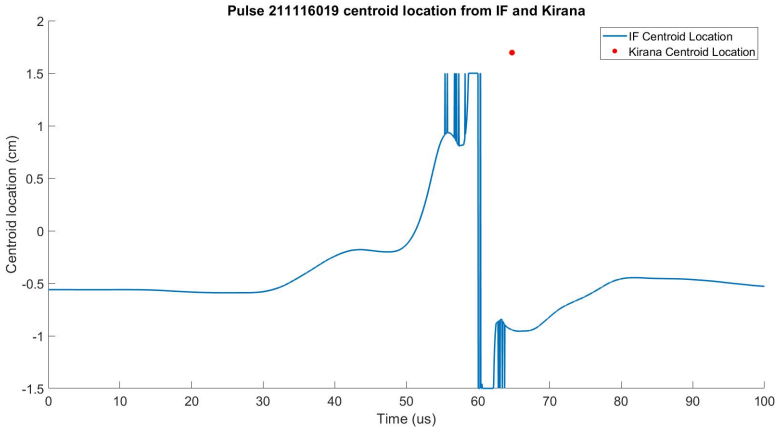

(a) Pulse 211116019

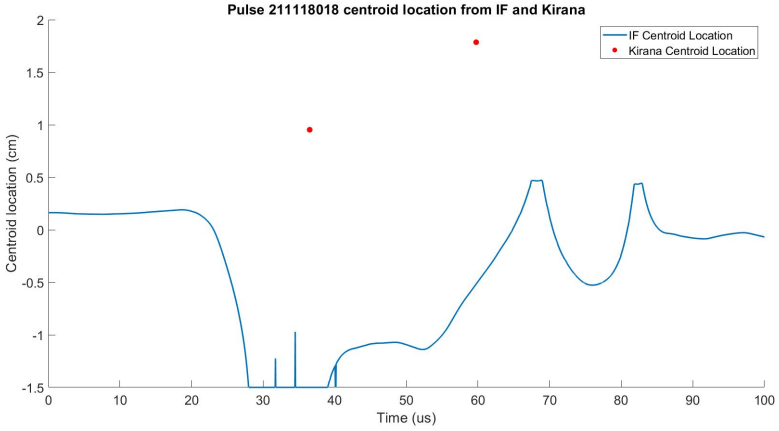

(b) Pulse 211118018

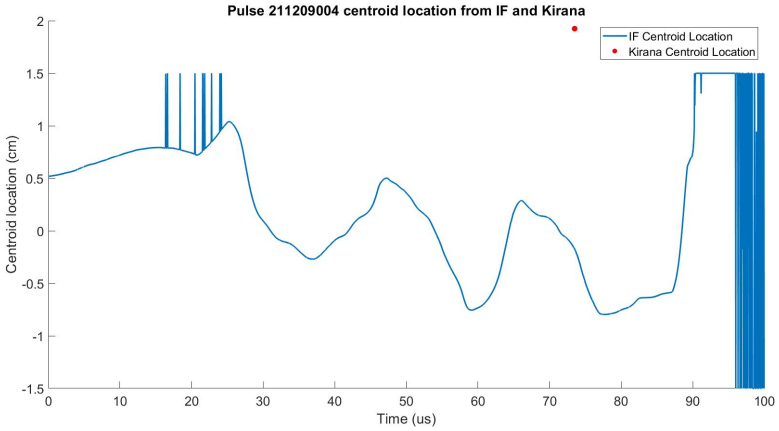

(c) Pulse 211209004

Figure 5.7: The above pictures show the traces of the interferometer centroid location along with the Kirana centroid data for the single time point.

Below is a table summarizing the centroid location between the Kirana and interferometer. The distances listed are solely measured along the y axis.

Table 5.4: This table outlines the difference between the centroid locations determined by the interferometer and the Kirana along the y axis at one specific frame.

Pulse	Time (μs)	Kirana (cm)	IF (cm)
211116019	64.75	1.67	-0.94
211118018	36.50	0.95	-1.5
211118018	59.75	1.79	-0.52
211209004	73.50	1.92	-0.17

The difference between the Kirana and the interferometer centroid location is approximately 2.35 ± 0.26 cm. This appears to be a significant number, but the small variation between the average is more important. As mentioned earlier, the Kirana needed to be adjusted to compensate for the interferometer mirrors being in the way. This caused the results to be skewed for the Kirana. The interferometry mirrors were located 1.5 cm above the center of the viewing window. The Kirana was able to see the mirrors in the lower third of the frames, meaning that it was approximately 2 cm above the center. Another thing to note was that the Kirana was kept horizontal during all frames, mitigating any further skewing issues. If we subtract this 2 cm from the Kirana data, then the new table would look like the one shown below.

Table 5.5: This table outlines the difference between the centroid locations determined by the interferometer and the Kirana with the rough corrections applied.

Pulse	Time (μs)	Kirana (cm)	IF (cm)
211116019	64.75	-0.33	-0.94
211118018	36.50	-1.05	-1.5
211118018	59.75	-0.21	-0.52
211209004	73.50	-0.08	-0.17

This gives a difference in centroid location now of 0.35 ± 0.26 cm. The Kirana and interferometer appear to align much closer together than before. If this is true, it could mean that the Kirana and interferometry diagnostics agree for these pulses. It is important to note, however, that this is a rough calculation and further testing should be done to confirm this.

5.3 Comparison of IF and B Field Probes

Interferometry tended to have results that were physically closer to the B field probes outputs than that of the Kirana. This may be due to the fact that the interferometry setup is limited to ± 1.5 cm while the Kirana is limited to ± 2.5 cm, thus allowing less room for error. Regardless, the interferometry data still tended to overshoot the B field data when it came to centroid location. In addition, the interferometer is generally unable to resolve centroid location when either the top or bottom chord is showing the maximum density, compared to the other two chords. The one promising piece of the analysis showed that the two diagnostics at least agreed on the direction of the pinch, whether that be in the -y or +y directions. Shown below are several plots derived from the density traces. Some of the same pulses from the Kirana/IF section will also be used for this section.

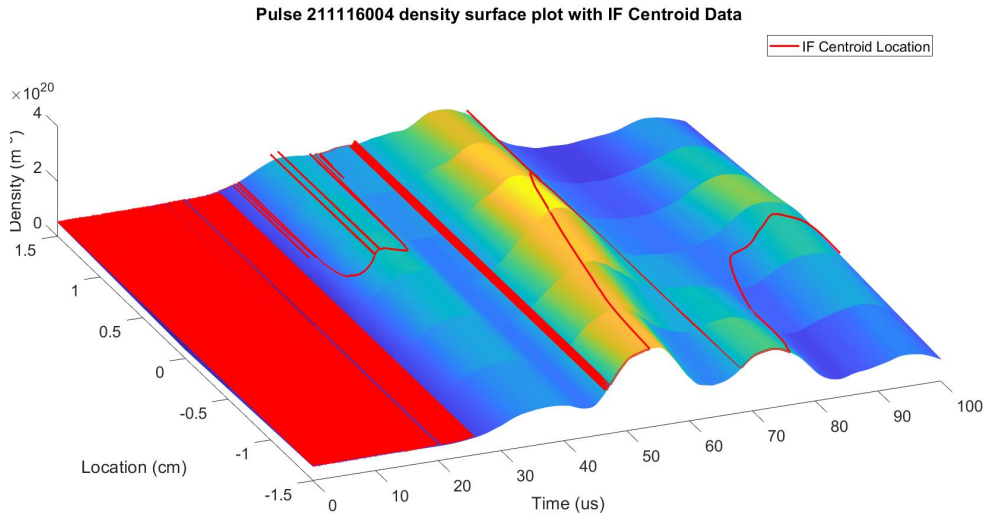

(a) Density Surface Plot with Centroid Location

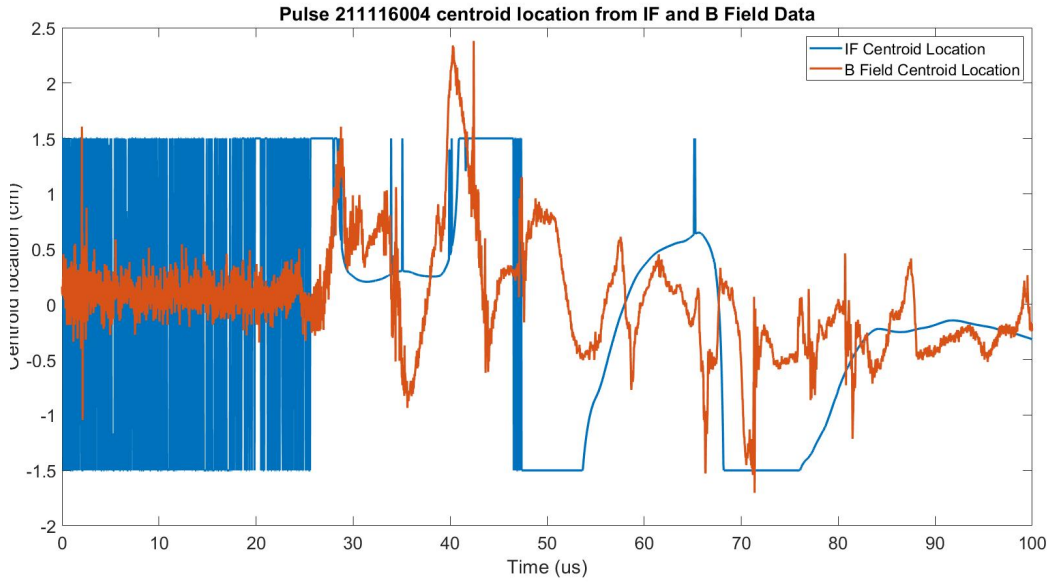

(b) Comparison of Centroid between IF and B Field Data

Figure 5.8: Centroid data for pulse 211116004

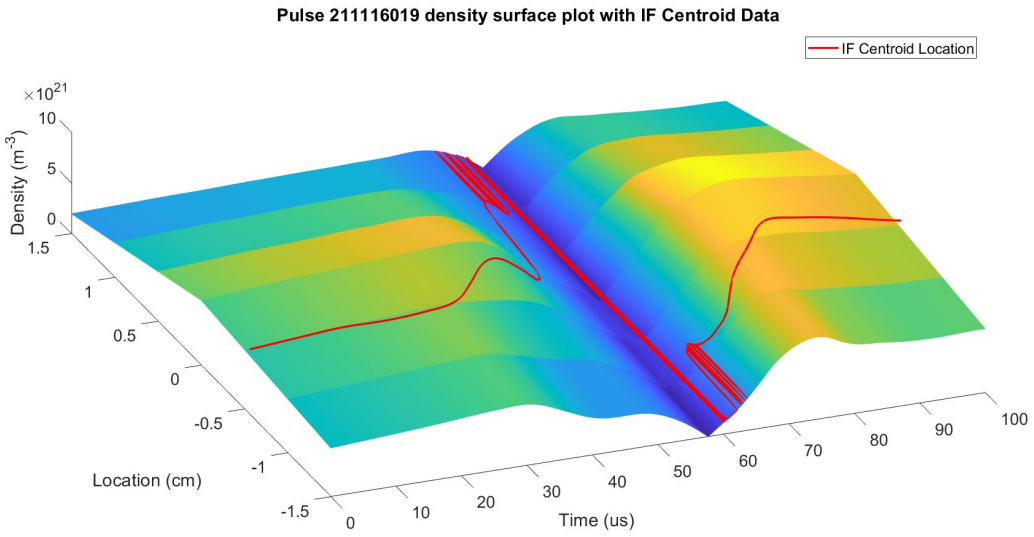

(a) Density Surface Plot with Centroid Location

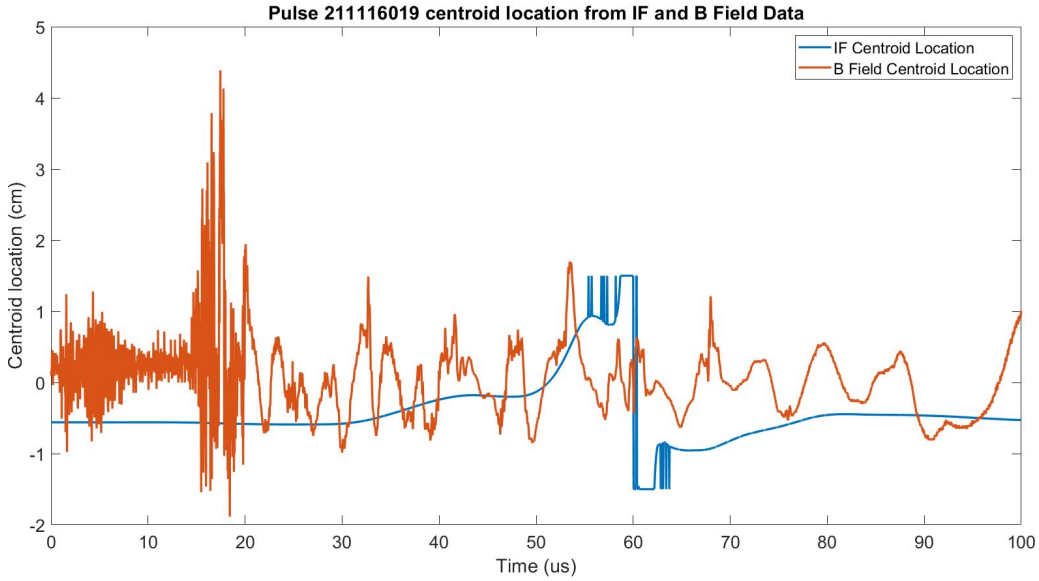

(b) Comparison of Centroid between IF and B Field Data

Figure 5.9: Centroid data for pulse 211116019

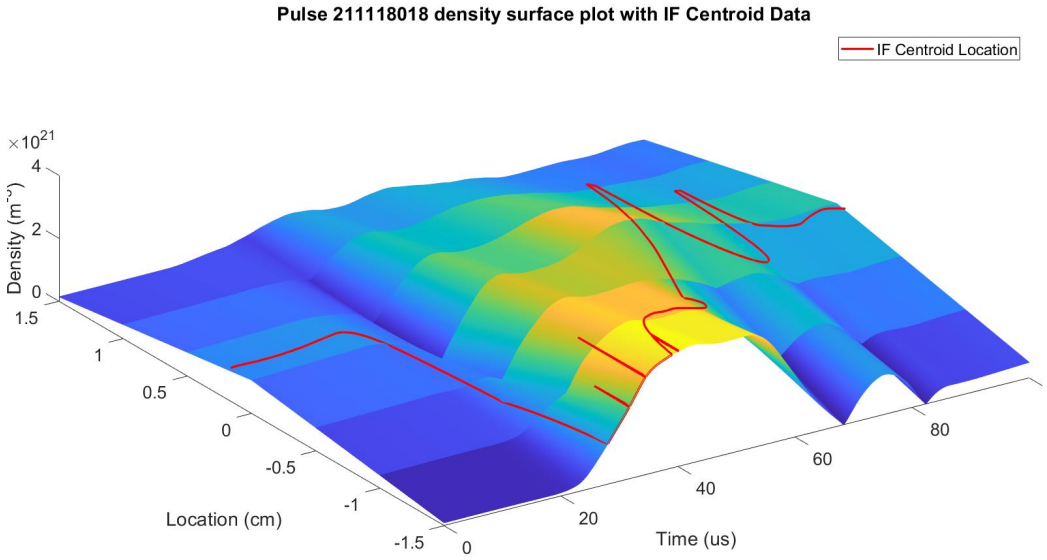

(a) Density Surface Plot with Centroid Location

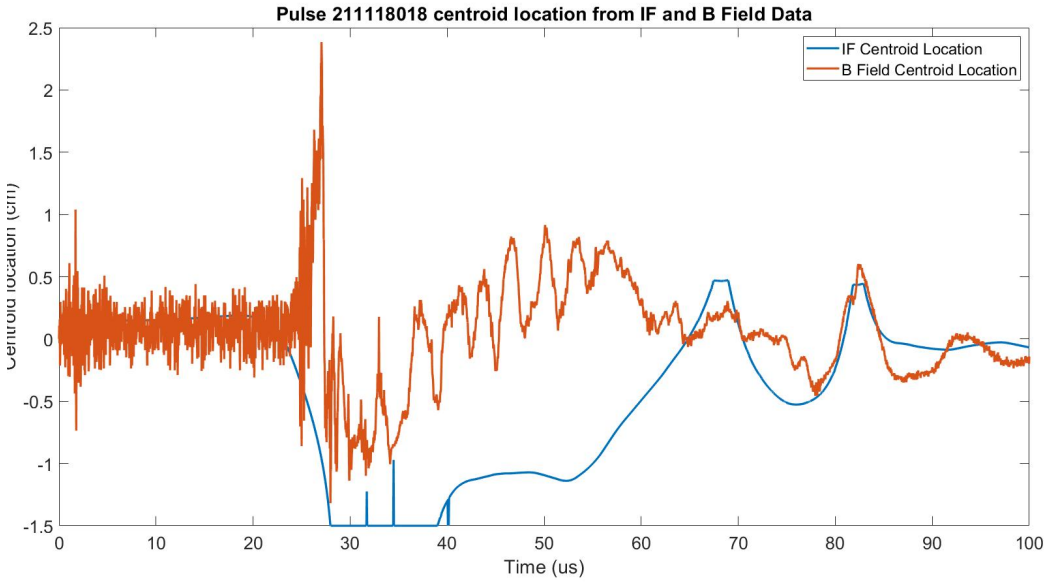

(b) Comparison of Centroid between IF and B Field Data

Figure 5.10: Centroid data for pulse 211118018

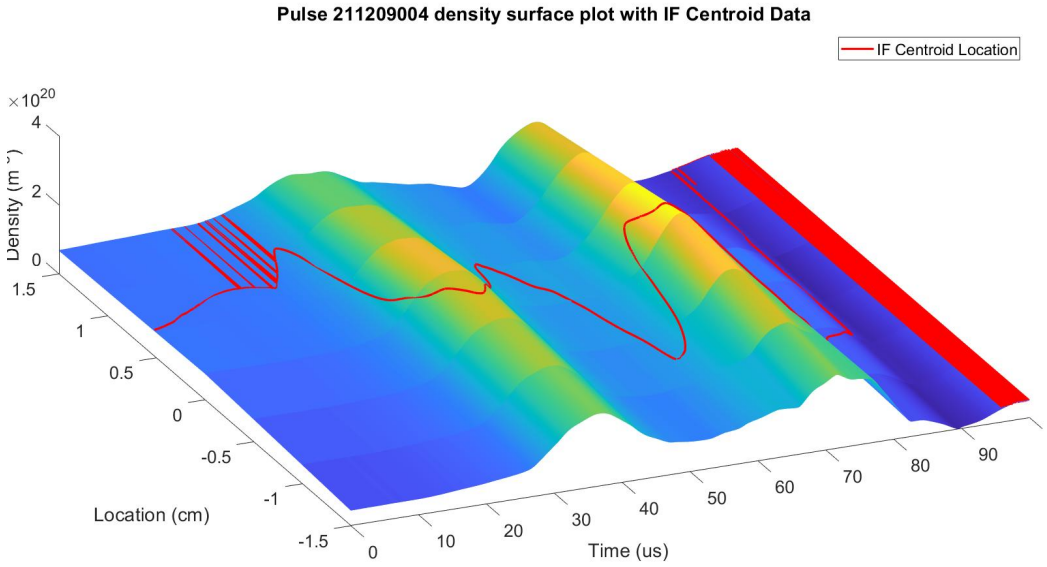

(a) Density Surface Plot with Centroid Location

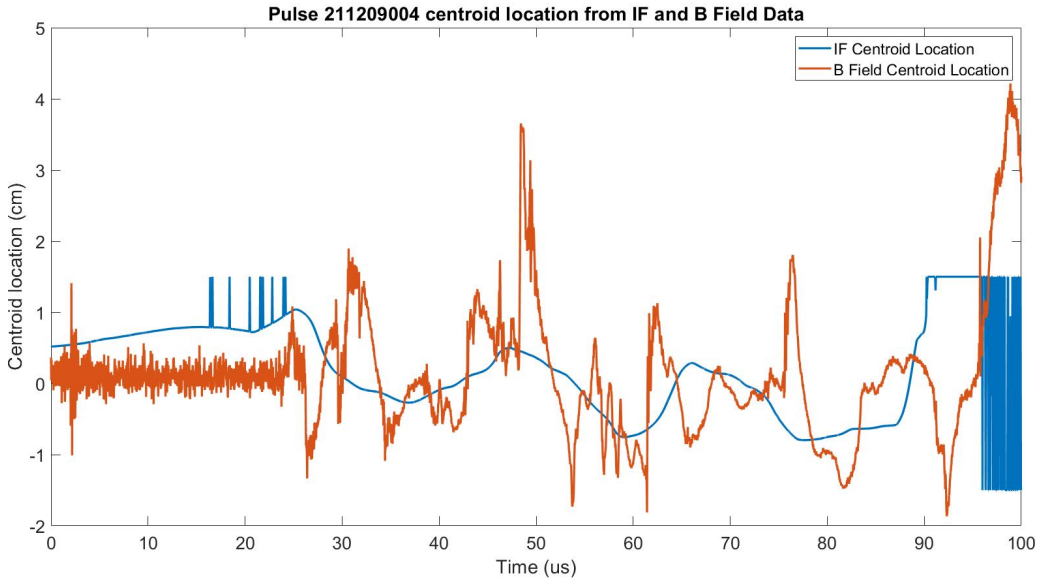

(b) Comparison of Centroid between IF and B Field Data

Figure 5.11: Pulse 211209004

For pulses where the center chord showed the highest density values, the two centroid traces tended to match up throughout the duration of the pinch. The interferometry trace however, tended to fluctuate slower than the magnetic field traces. This may be due to the smoothing algorithm used in the interferometry code, or the low pass filters used in the data acquisition system.

5.4 Comparison of all diagnostics

From section 5.2, we see that the Kirana data showed that the pinch was almost out of the viewing window, even for straight pinches. This was mainly due to the Kirana needing to be moved to accommodate the interferometer hardware. However, section 5.1 showed that for straight pinches, the magnetic field data and Kirana data only varied by at most one centimeter. For this section, it is assumed that the magnetic field centroid data is accurate for these pulses, and a one centimeter confidence margin has been implemented to account for the lack of good Kirana data. Below are plots showing the comparison between all three diagnostics. In implementing this assumption, any region where the interferometer centroid data crosses into the confidence margin implies that all three diagnostics agree on the location of the plasma centroid.

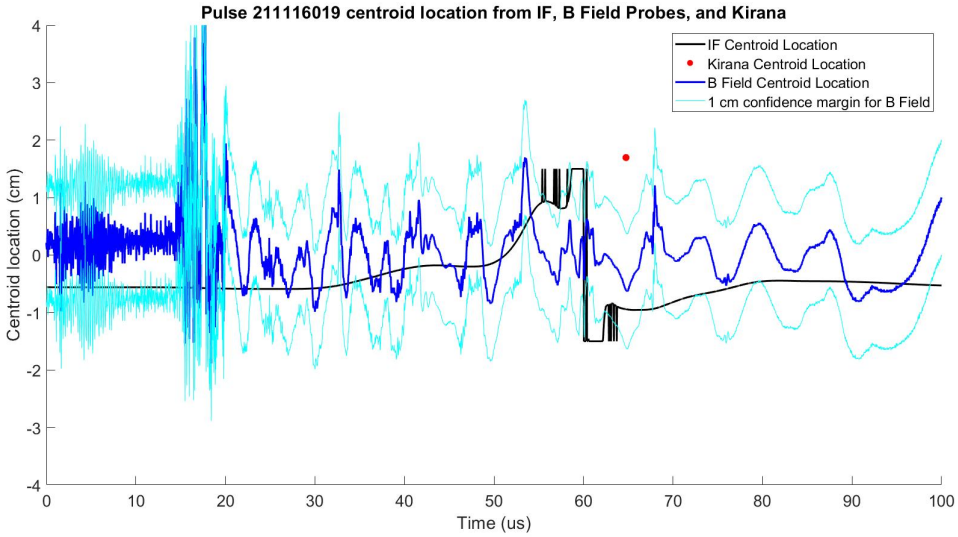

(a) Pulse 211116019

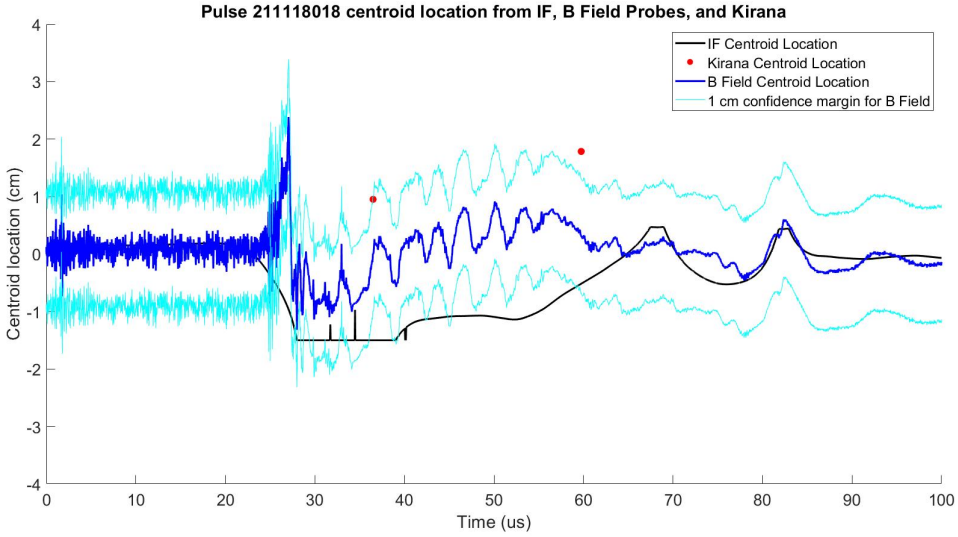

(b) Pulse 211118018

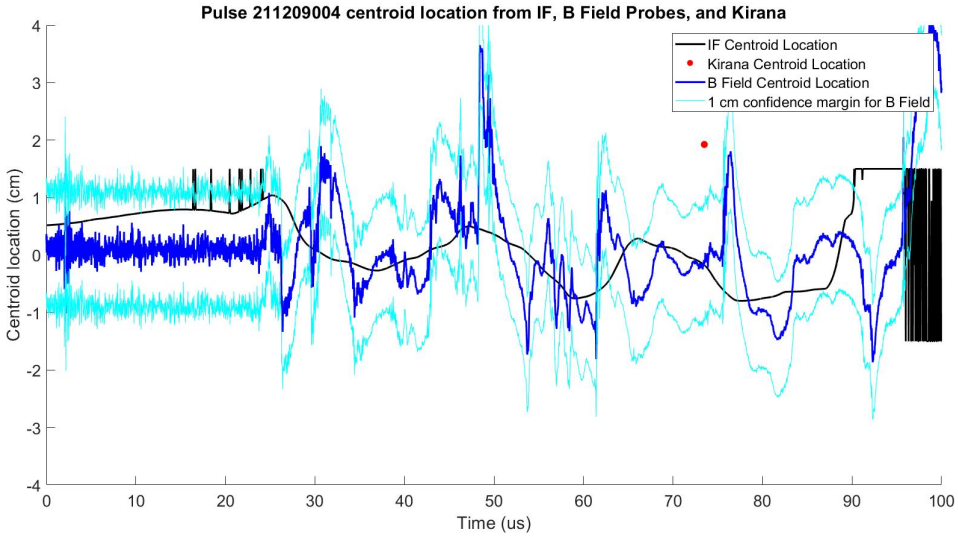

(c) Pulse 211209004

Figure 5.12: The above plots show the comparison between all three diagnostics in determining centroid location. The cyan traces are located at ±1 cm from the magnetic field trace (blue). They represent the confidence margin for possible centroid locations as calculated by the Kirana. These were included because the Kirana was not able to get a good view of the pinch with the interferometry hardware set up. In addition, the pinches chosen were straight and on-axis. For these pinches, the Kirana and magnetic field centroid locations tended to agree within one pinch radius.

Chapter 6
CONCLUSION

The ZaP-HD device is a Z pinch machine focused on proof of concept experiments in stabilizing and characterizing sheared flow stabilized Z-pinch plasmas. ZaP-HD is equipped with several diagnostic tools that can measure different characteristics about the plasma. The diagnostics used for this thesis include a Kirana fast-framing camera, a HeNe interferometer, as well as magnetic field probes.

The Kirana camera measures line emissions from the neutral hydrogen in the chamber. The output of the Kirana gives valuable insight into the shape, size, and position of the neutral cloud throughout the duration of the pulse. Using this information, and assuming that the plasma column is at the center of the neutral cloud, the Kirana is able to detect the centroid location of the plasma.

The interferometry diagnostic measures line integrated chord density of the plasma parallel to the chamber's x-axis. Three chords are placed at different heights in order to get both time and space resolved electron number density measurements at the P15 location. Using a combination of a Cauchy-Lorentz distribution function and MATLAB's built in optimization tools, a curve is fit to the three chords. This allows for time resolved centroid data from the interferometry diagnostic suite.

The magnetic field probes measure voltage probes through a loop of wire to determine the change in magnetic flux at that time. From this information, the absolute magnetic field strength can be determined, as well as mode and centroid location data.

6.1 Summary of experimental results

The comparison between the Kirana and the magnetic field probes included eleven separate pulses, separated into three sets. The first set of pulses were fairly straight and aligned onto the z-axis, while the second set of pulses were slightly unstable or off-axis. The third set

included must more unstable or ill-defined pinches. The Kirana was set perpendicular to the viewing window, centered at P15.

The interferometer was also centered at P15, with the three chords being located at $y = +1.5cm$, $y = 0cm$, and $y = -1.5cm$. When looking at the interferometry analysis, four pulses were analyzed. Typical peak density values ranged from $n_e = 10^{21}$ to $10^{23}m^{-3}$.

The magnetic field data was available for every pulse analyzed. Aside from a few peaks at the beginning and end of the quiescent period, the magnetic field probes reported the centroid generally staying within $\pm 1cm$ of the z-axis.

6.2 Summary of analysis

The Kirana data tended to overestimate the centroid location as compared to the magnetic field probes' outputs. For pinches that were relatively quiescent and without major instabilities, the Kirana yielded an average centroid position delta of approximately 0.85 cm. If the assumption that the centroid is located in the center of the neutral cloud holds true, the Kirana can be a viable tool for locating centroid locations in the future. The downside is that the magnetic field probe and Kirana data do not agree when pinches are no longer in the quiescent region.

The interferometer tended to yield results that were closer to the magnetic field centroid data than the Kirana. This may be due to the fact that the interferometer was more limited than the Kirana in terms of where it was able to measure in space. The interferometer diagnostic suite data loosely followed the magnetic field centroid data, but often had problems with the exact magnitude of the centroid and could not accurately discern pinches outside or near the boundaries of the top and bottom chords. As a result, the interferometer may be a viable tool for location the plasma centroid during quiescent periods. Outside of this, the interferometer in its current state falls short.

Putting all thee diagnostics together leads to some varied results. The most consistent tools to locate the plasma centroid were the Kirana and magnetic field probes. In times where the plasma is not quiescent, the Kirana may be the best current diagnostic for determining centroid location.

6.3 What to draw from analysis

In the quiescent period, where a pinch is centered and generally without instabilities, all three diagnostics work adequately for determining plasma centroid. Once minor instabilities set in, the interferometer, in its current setup, loses accuracy the quickest. It still however retains the ability to determine the general motion of the centroid through time. Once major instabilities set in, the magnetic field probes and the current code implemented lose accuracy. The Kirana seems to be the most consistent diagnostic tool throughout the duration of the pinch. However, it is subject to effects such as over saturation, ghosting, and reflections, making it susceptible to producing erroneous results if not set up properly. In addition, the Kirana does not have the accuracy nor the sampling rate that other diagnostic tools have. The magnetic field probe centroid data is accurate for pinches in the quiescent period since the assumptions have not been violated.

In the beginning of this paper, there was a discussion of attempting to combine data rich and data poor diagnostics together. At the current time, it seems that only data from the Kirana and magnetic field probes can be combined. The centroid data from these diagnostics matched up closely enough to where a Kirana may be able to take the place of the magnetic field probes at times. In addition, it may be possible to back out the magnetic field at the wall from equation 3.1 based solely on the centroid position determined from the Kirana. There are two main reasons why the Kirana and interferometry diagnostics are unable to be combined at this time. The first is that the code that calculates the raw density values has issues with phase jump corrections and trendline subtractions. This is why the discontinuities seen in some of the density surface plots exist. The other reason is that there appeared to be no glaring differences in visual data between pinches when the interferometer data showed differences in density data. It may be worth looking into correlating the pinch width, brightness, or wavelength to the plasma density.

6.4 Future Work

There are multiple areas of this research that can be expanded upon in the future to help better understand the diagnostics used.

6.4.1 Magnetic Field Probes

The current centroid data uses the assumption that the pinch wavelength is long compared to the radius of electrode walls. During periods where this assumption is violated, it may be helpful to see what the equations 3.2 and 3.3 yield for the centroid location. This would need to be coded into Python and would also need aid from the Kirana. As mentioned earlier, these equations rely on data from the entirety of the pinch. The Kirana can provide visual data and resolve the different instabilities and their modes appearing throughout the pinch.

6.4.2 Kirana

This project only looked at single image frames with the Kirana camera. Analyzing all frames over the entire pulse would enable direct comparison between the magnetic field probes and the interferometer, as this would now also be time resolved. In addition, the current code will need updates to make it more robust and flexible in attempting to analyze pinches. Currently, the code can only handle analyzing pinches that are bright, and have minimal stray plasma clouds and reflections. One suggestion would be to include a similar piece of code to what was used in determining centroid location in the interferometer diagnostic. A distribution function can be curve fit to each of the peaks from the raw Kirana data. Doing this may be computationally more expensive, but will benefit from being able to analyze the pinch at all axial locations with less errors.

6.4.3 Interferometry

The code that converts the detector signal into density data contains issues with resolving phase jumps and subtracting the trendline present in the data. This will need to be reworked in order to have higher fidelity outputs. Another possible avenue to improving the diagnostic suite would be to include a fourth chord in analysis. Doing so would both improve accuracy and range that the code could analyze.

BIBLIOGRAPHY

[1] The physics of the tokamak - the fusion power plant, Jun 2021.

[2] Amierul Aqil bin Khairi and Uri Shumlak. Graphite electrode characterization on the zap-hd sheared-flow-stabilized z-pinch device. Master's thesis, 2021.

[3] M G Haines. Fifty years of controlled fusion research. *Plasma Physics and Controlled Fusion*, 38(5):643–656, May 1996.

[4] Dorian A H Hanaor, Matthias H H Kolb, Yixiang Gan, Marc Kamlah, and Regina Knitter. Solution based synthesis of mixed-phase materials in the Li2TiO3 - Li4SiO4 system. *Journal of Nuclear Materials*, 456:151 – 161, 2014.

[5] Bonghan Kim. Multi-chord heterodyne quadrature interferometry measurement of the fuze sheared flow z - pinch plasma. 2018.

[6] Martin David Kruskal and Martin Schwarzschild. Some instabilities of a completely ionized plasma. 223, May 1954.

[7] US Departent of Energy. Doe explains...deuterium-tritium fusion reactor fuel.

[8] Shafranov. The stability of a cylindrical gaseous conductor in a magnetic field. *Soviet Journal of Atomic Energy*, 171, October 1956.

[9] Vitalii Shafranov. The initial period in the history of nuclear fusion research at the kurchatov institute. *Uspekhi Fizicheskikh Nauk - USP FIZ NAUK*, 171, 08 2001.

[10] U. Shumlak and C. W. Hartman. Sheared flow stabilization of the $m = 1$ kink mode in Z pinches. *Phys. Rev. Lett.*, 75:3285–3288, Oct 1995.

[11] U. Shumlak, R. Lilly, C. Adams, R. Golingo, S. Jackson, S. Knecht, and B. Nelson. *Advanced Space Propulsion Based on the Flow-Stabilized Z-Pinch Fusion Concept.*

[12] U. Shumlak, B. A. Nelson, E. L. Claveau, E. G. Forbes, R. P. Golingo, M. C. Hughes, R. J. Oberto, M. P. Ross, and T. R. Weber. Increasing plasma parameters using sheared flow stabilization of a z-pinch. *Physics of Plasmas*, 24(5), 2017.

[13] Uri Shumlak. Z-pinch fusion. *Journal of Applied Physics*, 127(20), May 2020.

[14] C. Thoma, D. R. Welch, and T. P. Hughes. Ballistic and snowplow regimes in j×b plasma acceleration. *Physics of Plasmas*, 16(3), 2009.

[15] M Yamada, A C Janos, Jr Ellis, G W Hart, F M Levinton, R M Mayo, D D Meyerhofer, M Mimura, R W Motley, Y Ono, and et al. Investigation of spheromak configuration generated by inductive methods in the s-1 device, Aug 1988.

[16] Y. Zhang, U. Shumlak, B. A. Nelson, R. P. Golingo, T. R. Weber, A. D. Stepanov, E. L. Claveau, E. G. Forbes, Z. T. Draper, J. M. Mitrani, H. S. McLean, K. K. Tummel, D. P. Higginson, and C. M. Cooper. Sustained neutron production from a sheared-flow stabilized z pinch. *Phys. Rev. Lett.*, 122:135001, Apr 2019.

Appendix A

WHERE TO FIND THE FILES

https://github.com/timlloyd97/ZaP-HD-Code

VITA

Tim Lloyd is a 2d Lt in the US Air Force. He will be attending pilot training at the conclusion of completing this degree. Any questions about this project can be directed to him at timothy.lloyd97@gmail.com.